Design and Development of a Wearable Inductive Textile Sensor to Monitor Back Movements

by

Astrid García Patiño

B.A.Sc., Universidad Iberoamericana, 2017

Thesis Submitted in Partial Fulfillment of the

Requirements for the Degree of

Master of Applied Science

in the

School of Mechatronic Systems Engineering

Faculty of Applied Sciences

SIMON FRASER UNIVERSITY

Fall 2020

Declaration of Committee

Name:	**Astrid García Patiño**
Degree:	**Master of Applied Science**
Thesis title:	**Design and Development of a Wearable Inductive Textile Sensor to Monitor Back Movements**
Committee:	**Chair:** **Jason Jiacheng Wang** Associate Professor, Mechatronic Systems Engineering
	Carlo Menon Supervisor Professor, Mechatronic Systems Engineering
	Helen Bailey Committee Member Lecturer, Mechatronic Systems Engineering
	Krishna Vijayaraghavan Examiner Associate Professor, Mechatronic Systems Engineering

Ethics Statement

The author, whose name appears on the title page of this work, has obtained, for the research described in this work, either:

a. human research ethics approval from the Simon Fraser University Office of Research Ethics

or

b. advance approval of the animal care protocol from the University Animal Care Committee of Simon Fraser University

or has conducted the research

c. as a co-investigator, collaborator, or research assistant in a research project approved in advance.

A copy of the approval letter has been filed with the Theses Office of the University Library at the time of submission of this thesis or project.

The original application for approval and letter of approval are filed with the relevant offices. Inquiries may be directed to those authorities.

Simon Fraser University Library
Burnaby, British Columbia, Canada

Update Spring 2016

Abstract

This thesis focuses on the design and development of a wireless and wearable platform that employs an inductive sensor to track trunk movements when the user bends forward. The inductive textile sensor was designed based on the anthropometrical dimensions of the trunk's lumbar area of a healthy female. The chosen shape of the sensor was a rectangular flat coil. The inductance behavior was investigated using theoretical calculations and simulations. Formulas developed by Grover and Terman were used to calculate the inductance to validate the inductive textile design. The simulations were used to analyze the change of the inductance when the area, perimeter, height, and width of the rectangle was modified, as well as the effect of the number of turns of the rectangular flat coil. Results from the theoretical calculations and simulations were compared. The inductive textile sensor was integrated at the lumbar section of a sleeveless garment to create a smart wearable platform. The performance of the smart garment was evaluated experimentally on a healthy participant, and it was shown that the designed sensor can detect forward bending movements. The evaluation scenario was further extended to also include twisting and lateral bending of the trunk, and it was observed that the proposed design can successfully discriminate such movements from forward bending of the trunk. An interference test showed that, although moving a cellphone towards the unworn prototype affected the sensor readings, manipulating the cellphone when wearing the prototype, did not compromise the capability of the sensor to detect forward bends. The proposed platform is a promising step towards developing wearable systems to monitor back posture to prevent or treat low back pain associated with poor posture.

Keywords: inductive sensor; textile sensors; nurses; low back pain; wearable smart garment; trunk posture

Dedication

To my family.

Acknowledgments

I would like to express my gratitude to my supervisor, Dr. Carlo Menon, for his guidance through my journey as a Master student. I would also like to thank members of the Menrva Research Group for their support and help. Finally, I would like to give a special thanks to my family who always supported me.

Table of Contents

List of Tables

List of Figures

List of Acronyms

SFU	Simon Fraser University
LAC	Library and Archives Canada
LBP	Low Back Pain
CCU	Coronary Care Unit
ICU	Intense Care Unit
TENS	Transcutaneous Electrical Nerve Stimulation
NSAIDs	Nonsteroidal Anti-Inflammatory Drugs
VAS	Visual Analogue Scale
E-Textiles	Electronic Textiles
IMU	Inertial Measurement Unit
ECG	Electrocardiography
LED	Light-Emitting Diode
EEG	Electroencephalography
PCB	Printed Circuit Board
PVA	Poly Vinyl Alcohol
FPCB	Flexible Printed Circuit Board
IC	Integrated circuit
NASA	National Aeronautics and Space Administration
LDC	Inductance to Digital Converter
I2C	Inter-Integrated Circuit
UART	Universal Asynchronous Receiver/Transmitter
MRI	Magnetic Resonance Imaging

Chapter 1

Introduction

The material of this chapter is excerpted, modified, and reproduced with permission from the following papers that I co-authored:

- A. García Patiño, M. Khoshnam, C. Menon. "Wearable Device to Monitor Back Movements Using an Inductive Textile Sensor". Sensors, vol. 20, no. 3, p. 905, 2020.
- A. García Patiño, C. Menon. "Inductive Textile Sensor Design and Validation for a Wearable Monitoring Device", article in preparation

Sections of this chapter have been adapted from the above papers to fit the scope and formatting of the thesis.

1.1 Research Objectives

Low back pain (LBP) is the most common work-related musculoskeletal disorder among healthcare workers, especially nurses. One of the most common activities performed by the nurses during their workday is forward bending, which has been linked to an increased incidence of LBP. Previous studies have tried to prevent and treat LBP using different methods such as patient education, wearable devices, motion capture systems, exercise, and more. Unfortunately, there is still much controversy about which method is the best to prevent and reduce the prevalence of LBP in nurses. However, for chronic LBP, improper body posture during patient care activities was determined as the most common cause [1]–[4]. Considering the relationship between body posture and LBP, it could be beneficial to monitor trunk movements and provide relevant feedback to the nurses during their activities at the hospital. Monitoring trunk movements can be achieved using

wearable wireless technologies capable of monitoring trunk movements during a normal workday indoors and outdoors. The smart garment presented in this thesis was designed to monitor trunk movements in real-time for extended periods of time while being comfortable and wireless. The technology chosen for developing such a smart garment was an inductive textile sensing module. Although resistive textile sensors have been used to monitor trunk movements, the developed garments have presented with disadvantages that could be overcome by using inductive textile sensors as an alternative solution. Consequently, the design and validation of a single inductive textile sensor were one of the objectives of this thesis. The other objective of this thesis was to develop a wireless and wearable device based on the designed inductive textile sensor to monitor forward bending and investigate its performance. To summarize, the objectives of this thesis are as follows:

Objective 1. Conceptualization of a new technology to monitor back moments using an inductive textile sensor.

Objective 2. Design and validation of an inductive textile sensor through theoretical calculations and simulations, in which the inductance is calculated based on the change in the dimension (perimeter, area, height, and width) of the sensor and the number of its wire loops.

Objective 3. Development of a wireless and wearable device using the designed inductive textile sensor and investigation of its performance in tracking forward bending while overlooking lateral bending and rotation.

Figure 1.1 shows the scope of this work. The final design of the inductive textile sensor was based on the anthropometry of a healthy human body and the inductance calculation from simulations. The resulting system included a smart garment based on the designed inductive textile sensor. A study with a single participant was conducted to investigate the performance of the smart garment.

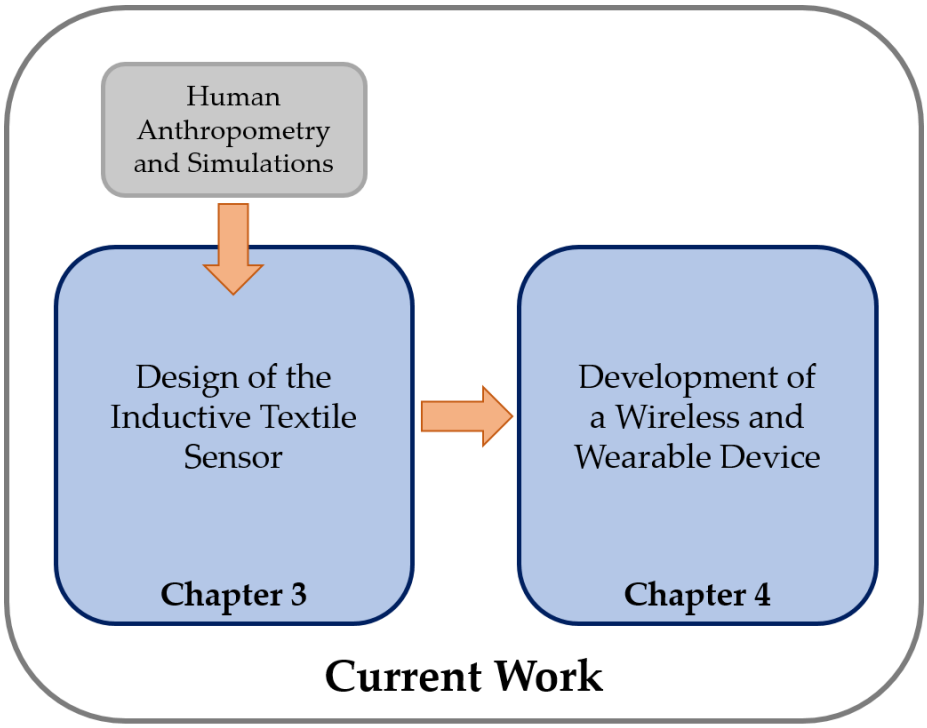

Figure 1.1. Thesis scope.

1.2 Motivation

Low back pain (LBP) is the most common work-related musculoskeletal disorder among healthcare workers [1]. In fact, half of all time-loss incidents in hospitals is due to back pain-related disability [2]. Hence, LBP is not only a social, ergonomic, health and, professional problem, but also an economic problem affecting individuals, families, communities, industry, and governments [3], [5]. Among healthcare workers, nursing is known to be the profession with the highest risk of LBP [1]–[3], [5], [6] with a prevalence of 35.9% in New Zealand, 47% in the United States, and 66.8% in the Netherlands [6]. Several studies confirmed the prevalence of LBP among nurses; e.g. Videman et al. [2] reported that after a follow-up of 7.5 years, back pain increased from 31% to 72% during nursing school. Nourollahi et al. [1] showed the prevalence of LBP was 29% in the general population, but 72% among nurses. Yip [4] revealed the annual incidence of LBP among

nurses was 39%, and Engels et al. [7] found the prevalence of low back complaints among nurses was 34%.

The high incidence of LBP in nurses can be explained by studying the activities they performed during the day. Most of those activities involved lifting and moving patients and manipulating materials (lifting, moving, carrying, and holding loads), which required a high level of physical capacity. Moreover, inadequate patient transferring devices, lack of appropriate methods to perform the mentioned activities, inappropriate layout of workstations, frequent back twisting and bending postures, and working in awkward positions made such tasks even more challenging [1]–[4]. Sedentary work, whole-body vibration, obesity, low body weight, poor fitness, low job satisfaction, lack of social support, insufficient adjustment for psychosocial work characteristics, poor relationships at work, stress, smoking, and hot conditions were also among factors associated with LBP [2], [4], [8]–[10].

Videman et al. [2] reported that working in twisted/bent postures was unquestionably associated with back pain and disability. However, they found an unclear association of physical loading in nursing with back pain and related disability. Nourollahi et al. [1] revealed an association between the exposure time holding an awkward trunk posture and LBP. Nourollahi et al. [1] also mentioned a difference in the physical workload between wards. The wards with higher median and peak trunk flexion angles of nurses were, in general, orthopedic and coronary care unit (CCU); while the ward more frequently exposed to high physical pressure was orthopedics, and the wards with the longest duration of exposure to awkward postures were, in general, orthopedics and intensive care units (ICU). One of the major conclusions of their study was that awkward postures were consequences of poor ergonomics in the wards. Yip [4] found several physical factors, such as bending to lift an object from floor level, handling patients, spending long periods of time in a single posture, and frequency of common work activities caused LBP. Yip [4] also reported that the psychosocial environment including being transferred to a new ward, and having poor work relationships with colleagues

were independent predictors of new LBP. Engels et al. [7] concluded that low back complaints seem to be associated with awkward postures, stooping, and lifting in nursing work, and they suggested focusing on symptoms in the associated anatomical sites for further investigation.

To reduce the prevalence of LBP among nurses, several techniques, methods, and treatments have been proposed, including [11]:

- **Physical treatments:** interferential therapy, laser therapy, lumbar supports, shortwave diathermy, therapeutic ultrasound, transcutaneous electrical nerve stimulation (TENS) and thermotherapy, and traction.
- **Exercise therapy**: type of therapy where participants are required to carry out repeated voluntary dynamic movements or static muscular contractions.
- **Manual therapy**: manipulation/mobilization and massage.
- **Education:** Back school, patient education, and McKenzie method.
- **Cognitive-behavioral treatment methods:** this type of method is focused on modifying environmental contingencies and cognitive processes.
- **Multidisciplinary treatment:** commonly, this type of treatment is a combination of physical, modification of medication, vocational, and behavioral components.
- **Pharmacological procedures:** antidepressants, muscle relaxants, Nonsteroidal anti-inflammatory drugs (NSAIDs), opioids, antiepileptic drugs, and capsicum pain plasters.
- **Invasive procedures:** acupuncture, injections, and nerve block surgery.

Despite the variety of techniques and methods, there is still much controversy about the best method to prevent and reduce the prevalence of LBP in nurses. However, for chronic

LBP, the most common cause is a general bad body posture or improper body postures such as slouching during patient care activities [1]–[4], [9], [10].

Therapies such as Back school, patient education, and McKenzie method have been helpful to improve body posture. Back school is an educational and training group program provided by therapists to prevent and reduce low back pain [12], while the McKenzie method therapy includes individual education and postural training components [13]. For example, one subset of this method, namely the postural syndrome, targets educating about the body posture [14]. Therefore, the McKenzie Method should be included in the therapies that improve body posture as long as pain due to poor posture is detected or if the therapy includes postural training.

Several studies suggested that education is effective in the treatment and prevention of LBP. Jaromi et al. [3] revealed that Back school had a long-term, i.e. 12 months, effect on decreasing pain since participants adhered to maintaining a good posture. Back school in combination with manual handling training resulted in a statistically significant reduction of LBP intensity compared to passive physiotherapy. Steffens et al. [15] reported that it is not possible to determine whether education alone can prevent LBP because of the low quality of evidence; nevertheless, education in combination with exercise is likely to reduce the risk of LBP. Furthermore, in longer-term follow-up, the combination of exercise with education was effective for the prevention of LBP episodes, while exercise alone was not [3], [12]. Straube et al. [12] found that back school showed an improvement in pain against exercises and a significant reduction in different self-report questionnaires to measure pain such as, Visual Analogue Scale (VAS) and in the Roland Morris Disability Questionnaire score. The systematic review conducted by Straube et al. [12] revealed that no firm conclusions can be drawn on which method is more effective when treating LBP because of the heterogeneity between the studies and the incomplete or lack of information reported within. Lam et al. [16] reported that the McKenzie method, including postural correction and education, resulted in a significant improvement in pain intensity compared to first-line care only. The McKenzie method also showed a significant

difference in pain after the intervention compared with exercise, combined manual therapy and exercise, and education. Moreover, a significant difference in disability was reported favoring the McKenzie method over the same aforementioned treatments. Lam et al. [16] concluded that the McKenzie Method was more effective in reducing pain and disability when the LBP was chronic. Finally, Murtezani et al. [13] found that the McKenzie method was superior to interferential current, ultrasound, and heat for pain relief and disability in the short-term, i.e. 3 months.

Considering the relationship between body posture and LBP, it could be beneficial to monitor trunk movements and provide relevant feedback to the nurses during their activities in the hospital. Previous studies collected such information using questionnaires [2], [7], [8], [10], [17]–[19], accelerometers [1], [9], [20]–[22], and other type of technologies such as optical motion-tracking systems [18], [23], [24]. These solutions have limited practicality since questionnaire results might be subjective, data collected with accelerometers might be inconsistent due to sliding, accidental removal of sensors, skin movement, or misalignment between the sensor axes and underlying anatomical segments [25], and cameras and similar motion-capture systems are bulky with long setup times that can be accommodated mostly in dedicated clinical environments.

Fortunately, electronic textiles (e-textiles) or smart garments provide a viable wearable solution for developing standalone platforms that can objectively monitor back movements. In such systems, electronic components and/or textile sensors such as inertial measurement units (IMUs), capacitive, resistive or inductive sensors, and light-emission diodes (LEDs) are embedded within the fabric [26]–[29]. Some of the applications of such platforms in healthcare are electrocardiography (ECG), sports research, plethysmography, postural monitoring, movement analysis, and muscle activity measurements [26], [29], [30]. E-textiles have also been considered in developing wearable and comfortable movement tracking platforms due to their small size, lightweight, and simple operation that allows for unobtrusive monitoring of user movements during activities of daily living [27], [31].

Acknowledging these important advantages, the prominent types of textile sensors that have been investigated as possible solutions are:

- **Resistive textile sensors**
- **Capacitive textile sensors**
- **Inductive textile sensors**

In healthcare, only resistive textile sensors have been successfully used in wearable platforms for back posture monitoring [31], [32], [33]. The disadvantages that limit the resistive textile sensors practicality are high hysteresis, non-linearity response, and drift in their readings [33]. In the past studies that have used inductive sensors reported a linear behavior, reduced hysteresis in comparison with the resistive sensors, no drift, and simple manufacturing process [34]–[39]. Therefore, inductive textile sensors could be a potential solution for back posture monitoring to prevent and treat LBP. Tormene et al. [32] highlighted the challenges in discriminating between different movements, such as forward bending and lateral bending. Therefore, the motivation of this thesis was to design and develop a wireless smart garment based on a single inductive textile sensor that can monitor forward bending and distinguish forward bending from other trunk movements such as lateral bending and rotation. Considering practicality, the developed system should be a lightweight and comfortable wearable platform with a long battery life that can last a work shift. Such a system is well-suited for objective monitoring of forward bending of the trunk.

1.3 Scientific Contributions

This thesis contributes to the advancement of wearable health monitoring devices by developing a novel wireless and wearable device to monitor the trunk's movements. Firstly, a new inductive textile sensor was designed, studied, and developed. The research and design process of the sensor led to an understanding of how the inductance was

affected by changing two parameters: 1) the height, width, perimeter, and area of the sensor, and 2) the number of loops in the inductive textile sensor. The inductive textile sensor was shown to be capable of detecting small strain differences on the fabric. Secondly, a smart garment was prototyped to monitor forward bending using the designed inductive sensor. Thirdly, the advantages and disadvantages of using the inductive textile sensor in wearable health monitoring devices were discussed. The introduced research generated the following academic journal publications:

- A. García Patiño, M. Khoshnam, C. Menon. "Wearable Device to Monitor Back Movements Using an Inductive Textile Sensor". Sensors, vol. 20, no. 3, p. 905, 2020.

- A. García Patiño, C. Menon. "Inductive Textile Sensor Design and Validation for a Wearable Monitoring Device", article in preparation

1.4 Outline

The thesis is organized as follows:

Chapter 2. This chapter introduces the concept of e-textiles, different types of textiles sensors (e.g. resistive, capacitive, inductive sensor), and their integration into the fabric.

Chapter 3. In this chapter, the inductive textile sensor was designed based on the anthropometry of the human body. The inductive sensor was theoretically and experimentally studied to understand inductance behavior. For calculation purposes, the inductive textile sensor in the shape of a flat rectangle coil was simulated to study how the inductance value changed when different parameters were modified, such as perimeter, area, weight, height, and the number of loops in the sensor.

Chapter 4. This chapter describes the development of the smart garment using the designed inductive sensor. The proposed prototype was a wireless, comfortable, and compact textile-based wearable platform to track trunk movements when the user bends forward. The evaluation of the smart garment's performance was done by asking a healthy participant to wear the instrumented garment and perform several repetitions of forward bending, lateral bending, and trunk rotation. Furthermore, a magnetic interference test was used to investigate the behavior of the inductive sensor in proximity of other objects, such as a magnet, metallic objects, and wireless devices.

Chapter 5. This chapter concludes the thesis with and overview of objectives, results, and directions for future research.

Chapter 2

Background

2.1. E-Textiles

E-textiles, also known as “Smart Fabric”, “Functional Apparel” and “Wearable Technology” are textiles in which the fabric is instrumented with any type of technology that conducts electricity. Examples of such technologies include wires, sensors, conductive materials, batteries, circuitry boards, and light-emitting diodes (LEDs) [26], [29], [40]. E-textiles are mostly used for electromagnetic shielding, anti-static, heating purposes, and soft circuits which combine special fabrics, threads, and yarns with electronic components [41]. Some of the key functionalities of e-textiles are stretchability, flexibility, conductivity, heat regulation, luminescence, response to touch, and sensing [28], [42]. These functionalities make the e-textile potentially useful in fields like healthcare, sports, military, gaming, and space exploration. In healthcare fields, some of the most relevant applications are electrocardiography (ECG), electroencephalograms (EEG), sport research, plethysmography, measurement of body temperature, postural monitoring, movement analysis, and muscle activity measurements [26], [28], [29], [31], [41], [43], [44].

E-textiles could be a solution for monitoring daily activities, not only because they perform the previously mentioned functionalities, but also due to their small size, lightweight, and simple operation [27], [31]. As a result, they can comfortably be worn by participants without obstructing their daily activities.

Commonly, the soft circuit e-textile consists of flexible or small electronics, and conductive materials to transmit the signals and power. The most common electronics are rigid or flexible printed circuit boards (PCBs), textile-based sensors, small batteries (usually

Lithium Polymer), connectors, electrodes, and conductive thread. While flexible conductive yarns, non-conductive coated yarns with metals (usually stainless steel or conductive silver with nylon core), galvanic substances or metallic salts, conductive inks, and carbon nanotubes are normally used to supply power to the circuitry or transmit signals between the electronics [26], [28], [41], [43].

Textile-based sensors have slowly been introduced into wearable devices due to their small size, practicality, and simplicity of use [27], [28]. Textile-based sensors are described as modules that measure and convert a mechanical input into an electrical signal that can be interpreted as a capacitive, resistive, or inductive value.

2.1.1. Resistive Textile Sensors

Resistive textile sensors are made in a variety of shapes with various production techniques, such as incorporating conductive threads (e.g. carbon nanotubes, silver-coated thread) into textiles using sewing, embroidery, weaving, knitting, or braiding machines. Coating non-conductive threads with a conductive material and printing conductive inks (e.g. metals, galvanic substances, metallic salts) into the textile are other production techniques [27], [28]. The fundamental working principle of resistive sensors is that any mechanical deformation of the sensor results in a change in its electrical resistance [30], [31], [42].

In previous studies, resistive textile sensors have been used to detect ECG, respiration, body posture, movement, and humidity. Pacelli et al. [45] presented two techniques for manufacturing resistive sensors: one based on knitting and the other based on printing. The knitted sensor was used to detect respiration and bending of the elbow. The printed sensor was tested for movement and posture detection. Rezaei et al. [30] developed a smart sleeveless shirt for measuring the kinematic angles of the trunk. Huang et al. [46] created a smart shirt using printed electrodes capable of detecting ECG and respiration. Tormene et al. [32] presented a smart garment to monitor movements of the back using

printed resistive sensors. Liao et al. [47] developed a flexible and highly sensitive resistive sensor capable of measuring tension and compression. Esfahani et al. [31] presented a trunk motion tracking system by using a printed resistive sensor. Zhou et al. [42] fabricated a textile-based humidity sensor by using polyvinyl alcohol (PVA) polymer filaments; the resistance value of which changed depending on the humidity. Gholami et at. [48] fabricated a prototype with 9 fiber strain sensors to kinematic monitoring of runners. Figure 2.1 illustrates an example of a smart garment with resistive textile sensors embedded.

Figure 2.1 Example of a smart garment with resistive strain sensors [48]. This image is licensed under a Creative Commons Attribution license (CC BY). Source image: Gholami, M.; Rezaei, A.; Cuthbert, T.J.; Napier, C.; Menon, C. Lower Body Kinematics Monitoring in Running Using Fabric-Based Wearable Sensors and Deep Convolutional Neural Networks. *Sensors* 2019, *19*, 5325, https://www.mdpi.com/1424-8220/19/23/5325. Accesses on 20/September/2020.

Unfortunately, resistive textile sensors are characterized by high hysteresis, non-linearity of their response, and a drift in their readings when a certain amount of stretch is held for a period of time [27], [49].

2.1.2. Capacitive Textile Sensors

Capacitive textile sensors are formed by two or more conductive plates and a dielectric element. Conductive plates can be fabricated through different methods, such as sewing, embroidering, or weaving conductive material such as conductive threads into the fabric and coating or painting a section of the textile with conductive ink [28]. Another method uses conductive polymers as the conductive plates attached to the textile [27]. The dielectric component required between the conductive plates can be made using soft non-conductive polymers, foams, or fabric spacers [28]. The fundamental working principle of capacitive sensors is that the capacitance value depends on the distance between the conductive plates. In other words, when conductive plates become closer to each other as a result of applied pressure, the capacitance value increases. In comparison with resistive textile sensors, these sensors demonstrate more linear behavior, less hysteresis, and faster response time [27], [28]. The manufacturing process of capacitive sensors is more complicated and requires more equipment than that for resistive sensors [27].

Capacitive textile sensors have been previously used to track motion and measure torsion, pressure, strain, and touch [27], [44], [49]–[51]. Atalay [27] developed a capacitive strain sensor for tracking the motion of the knee joint where the sensor was made using silicone and conductive fabric. Chhetry et al. [50] presented a highly sensitive and durable capacitive pressure sensor based on a microporous dielectric material. Cooper et al. [51] prototyped a capacitive double helix sensor capable of measuring strain, torsion, and touch. This sensor was made by using filaments composed of hollow elastomeric capillaries filled with liquid metals. Seung-Rok et al. [44] manufactured an interdigitated capacitive strain sensor used to detect finger and wrist muscle motions. Figure 2.2 shows an example of a capacitive textile sensor.

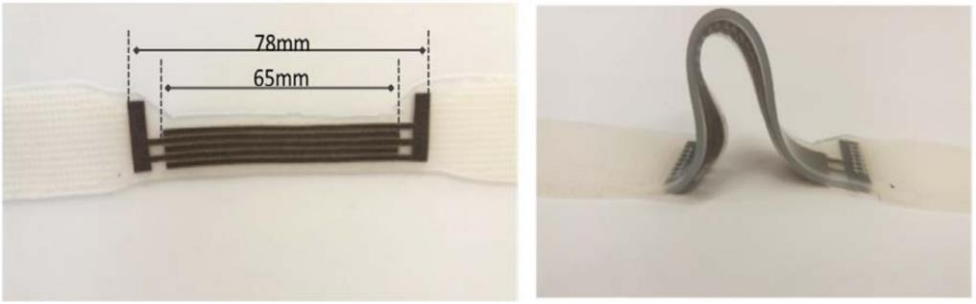

Figure 2.2 Example of a capacitive textile sensor [27]. This image is licensed under a Creative Commons Attribution license (CC BY). Source image: Atalay, O. Textile-Based, Interdigital, Capacitive, Soft-Strain Sensor for Wearable Applications. *Materials* 2018, 11, 768, https://www.mdpi.com/1996-1944/11/5/768/htm. Accesses on 20/September/2020.

2.1.3. Inductive Textile Sensors

Inductive textile sensors are made from highly conductive materials, such as copper wire, stainless steel yarn, or conductive threads that combine different alloys. The working principle of these sensors is that an electrical current is passed through loop(s) of conductive threads to create a magnetic field. Sensor deformation due to an externally applied force affects the shape of the magnetic field and, thus, changes the sensor output. Consequently, it is possible to increase the inductance and sensitivity (Δ Inductance$/\Delta$ strain) of the sensor through augmenting the number of coils and/or narrowing the width and space between the coils [52]. Inductive sensors typically have a loop configuration with a circular geometry, although they might also be manufactured in other shapes such as a square, rectangle, and pentagon [53]. The possibility of manufacturing inductive sensors in various shapes grants them the versatility to be embedded in or affixed to different surfaces. Consequently, inductive sensors are regularly used in antennas [54], [55] and plethysmographs [35], [53], [54].

Yoo [40] and Coosemans et al. [36] used inductive-type of sensors for wireless-powered applications. Coosemans et al. [36] created a platform using this type of sensor to transmit ECG measurement data. To measure the heartbeat, Koo et al. [38] developed a magnetic-

induced conductivity sensing module shaped in a coil configuration using nine strands of silver-polyester hybrid yarn. Wijesiriwardana [37] manufactured a knitted sensor made with Lycra and copper wire to measure strain and displacement, suggesting the possibility of expanding the sensor's applications to respiration measurment and motion and gesture capturing systems. This sensor was reported to be ideal for wearable devices given its unobtrusive behavior, small size, lightweight, comfortable and tightfitting properties. Wu et al. [56] presented a wearable inductive plethysmography to monitor respiration during sleep. This inductive plethysmography showed high reliability with low production cost. Tavassolian et al. [39] developed a wearable device to monitor multiaxial hip movement using inductive soft strain sensors. Huang et al. [57] created a stretchable wireless sensor to monitor cutaneous strain/pressure using copper film to create a resonant circuit. Bonroy et al. [58] presented an inductive sensor to monitor knee flexion and extension. Sardini et al. [34] developed a wearable device to monitor the posture of the spine using two inductive sensors. Figure 2.3 illustrates an example of a smart garment with four inductive textile sensors embedded.

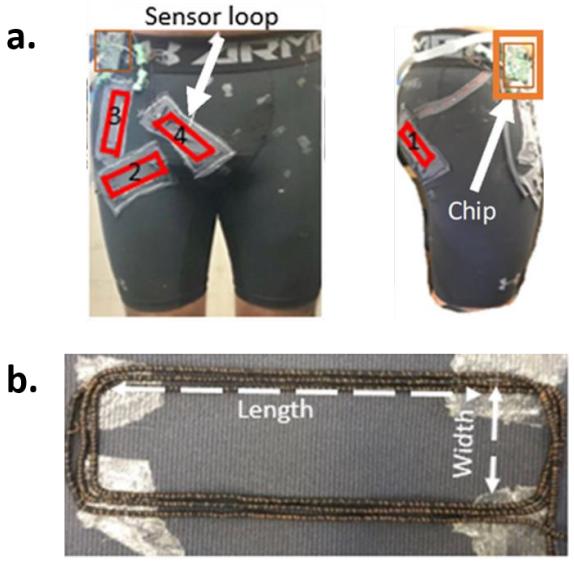

Figure 2.3 Example of a smart garment with four inductive textile sensors embedded [39]: (a) front and lateral view of the smart garment; (b) inductive textile sensor attached to the fabric. This image is licensed under a Creative Commons Attribution license (CC BY).

Source image: Tavassolian, M., Cuthbert, T.J., Napier, C., Peng, J. and Menon, C. (2020), Textile-Based Inductive Soft Strain Sensors for Fast Frequency Movement and Their Application in Wearable Devices Measuring Multiaxial Hip Joint Angles during Running. *Adv. Intell. Syst.*, 2: 1900165, doi: 10.1002/aisy.201900165, https://onlinelibrary.wiley.com/doi/abs/10.1002/aisy.201900165. Accesses on 20/September/2020.

A difference between resistive and capacitive textile sensors is that the manufacturing process of the inductive textiles sensors does not require specialized equipment or materials. Commonly, these type of sensors have been fabricated using copper wire of different dimensions [34]–[37], [39], [55], [57]. Similar to other textile sensors, the inductive textiles sensors can be easily integrated into the garments without causing discomfort or being obtrusive. An advantage of inductive textiles sensors is the possibility to easily manufacture them in different shapes and dimensions, whereas resistive and capacitive textile sensors are limited to a size and shape. Increasing the size and/or number of loops of the inductive textile sensor increases their output signal sensitivity [37], [39], [52]. However, increasing the number of loops of the inductive sensor may also increase the stiffness of the garment causing discomfort to the user. A difference compared to resistive textile sensors or gyroscopes is that inductive sensors do not present a drift in their output signal over time, which makes them a reliable monitoring system for an extended period of time. Additionally, inductive textile sensors output signals present minimal noise, almost linear behavior, almost no hysteresis, and straightforward signal processing when compared with other devices (e.g. triaxial accelerometers, IMUs) [39], [58]. Finally, the output signal of the inductive sensors may be affected when a ferromagnetic element is in close proximity to the sensor causing noise and/or wrong measurements.

2.2. Integration of Textile Sensors into a Garment

The integration of textile-based sensors, conductive yarns, or non-conductive coated yarns into a garment or fabric can be done with various techniques. Some popular examples are

sewing, gluing, embroidering, embedding, weaving, knitting, coating, or printing [28], [43].

The objective of the coating process is to transform a non-conductive yarn into a conductive yarn using materials such as metals, galvanic substances, and metallic salts. Examples of coating methods are electrolysis plating, chemical vapor deposition, sputtering, and coating with a conductive polymer [28]. It is crucial that the coating is uniform, otherwise, the sensor may perform poorly [42]. Despite this disadvantage, previous studies have reported positive results using different types of fabrics and yarns coated with conductive materials [29], [41], [59], [60].

The embedding technique allows the integration of textile-based sensors, conductive yarns, or non-conductive coated yarns into the fabric during the manufacturing process. This advantage allows for the possibility of selecting the best stitch for each type of fabric [41], [61]. Some popular stitches used for stretchable fabrics are zigzag, curve, wave, and sinusoidal pattern. Sewing textile sensors into the fabric or garment presents several advantages such as geometry versatility, manufacturing ease, and the ability to replace the sensor without damaging the garment or fabric.

The embroidery technique has been used in previous works to develop an antenna to transmit data and power to a wearable electronic, where the antenna was made by directly sewing stainless steel yarn into the fabric in a spiral configuration [36], [54], [55].

In the knitting technique, textile-based sensors are created with a flat-bed knitting machine using either interlocking or plain knitted structures. These sensors have advantages of conforming to the shape of the body as well as improved elasticity and breathability [41], [43]. This technique can be done with a variety of conductive yarns, such as silver-coated nylon yarns, polyester-blended yarn with stainless steel fibers, and double covered elastomeric yarns [41], [43], [54], [60].

Finally, one of the most popular techniques is printing or stamping conductive ink into the fabric. The conductive ink can be prepared using a single conductive material or by combining several conductive materials such as silver, gold, and conductive elastomers [28]. Previous studies have used a flexible printed circuit board (FPCB) and an integrated circuit (IC) chip to design a garment for monitoring physiological signals such as ECG, heart rate, respiration signal, respiration rate, acceleration, and temperature. Printed resistive sensors have also been used for monitoring physiological signals [31], [32], [45]. The principal advantages of the printing technique are producing sensors that are comfortable, lightweight, low cost (relative simple industrial printing process), and incorporated into usable fabrics.

Overall, e-textile technology has shown the potential to overcome the current technologies' disadvantages. Such technology allows for fabricating wearable platforms that are comfortable and aesthetically pleasing while being able to measure different imported physiological signals throughout the day. In healthcare, this technology has been used in tracking back posture [30]–[33] with positive results highlighting the potential of e-textiles for these applications. Therefore, when considering the advantages of this technology, the e-textiles can provide information about the back movements of nurses during their activities, which is key to prevent and treat LBP.

Chapter 3

Sensor Design and Validation

The material in this chapter is excerpted, modified, and reproduce with permission from the following papers that I co-authored:

- A. García Patiño, M. Khoshnam, C. Menon. "Wearable Device to Monitor Back Movements Using an Inductive Textile Sensor". Sensors, vol. 20, no. 3, p. 905, 2020.
- A. García Patiño, C. Menon. "Inductive Textile Sensor Design and Validation for a Wearable Monitoring Device", article in preparation

Sections of this chapter have been adapted from the above papers to fit the scope and formatting of the thesis.

3.1. Introduction

This chapter investigates the design of the inductive textile sensor. The design of the sensor was initiated by defining the dimension of the lumbar section of a healthy participant. Such dimensions were set as the highest possible size of the inductive textile sensor. The design of the sensor was divided into two steps. First, the inductance value of the sensor was theoretically calculated using equations from the literature to understand the behavior of the inductance when a change in the geometry of the sensor occurred. Furthermore, a comparison between different theoretical calculations based on perimeter/area and height/width of a single loop rectangle was performed. For the second step, a series of simulations were investigated to verify the values obtained from theoretical calculation. In addition, the impact of including variables such as the material of the sensor and its surrounding environment was studied through simulations.

As discussed in the previous chapter, sewing is an effective method to integrate smart textiles into the garment. Therefore, in this thesis, sewing using a zigzag pattern was the chosen method to integrate the sensor into the garment. However, in theoretical calculations and simulations, the sensor was treated as a straight line, instead of a zigzag pattern to simplify the calculations and reduce the computational time. In previous studies, copper wire was integrated into garments to create inductive textiles sensors with promising results [36], [37], [40]. Therefore, the sensor's material selected for the studies presented in this thesis was a single thread of round copper wire of 0.14 mm diameter due to its excellent conductivity.

3.2. Anthropometry

The focus of this study was to detect forward bending of the trunk while rejecting other movements, such as lateral bending or twisting. To achieve this goal, the configuration and placement of the sensor was chosen strategically. Previous studies reported that when an individual wearing a tight-fitting shirt bends forward, the lumbar section of the back undergoes major strain [33]. The trunk movements in the frontal and horizontal planes, which correspond to lateral bending and rotation, cause a smaller strain on this section [33]. According to this evidence, the inductive textile sensor was positioned on the lumbar area, using a flat rectangle coil shape.

Given that more than 90% of nurses are female [62]–[64], the anthropometry of a healthy female was used as the reference in designing and testing the inductive textile sensor developed in this thesis. The general trunk's anthropometry dimensions of a healthy female using 95th percentile [65] and from recruited participants reported by previous studies [66]–[68]. The collected measurements are summarized in Table 3.1 and illustrated in Figure 3.1.

Table 3.1. Anthropometry dimensions of a healthy female of 25-40 years old.

Trunk's Anthropometry	
Trunk width at the iliac crest	28 cm
Trunk Length C7-L5	41.7 to 42.5 cm
Waist Height	103.4 cm
Trochanteric Height	82.4 cm

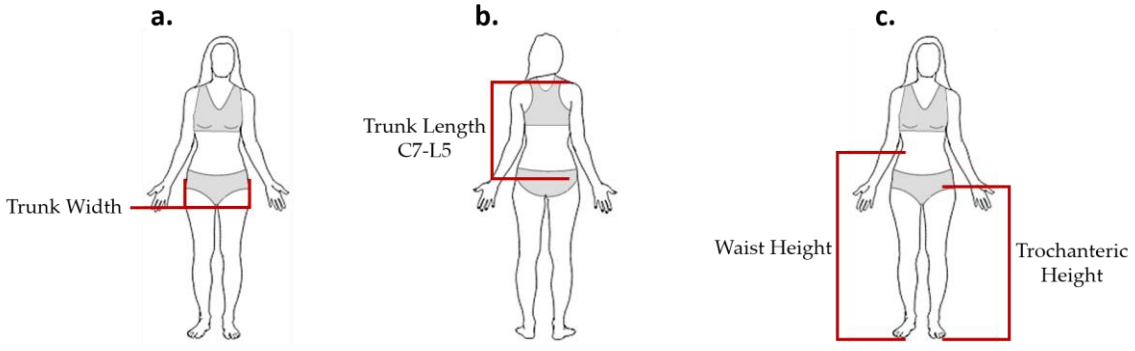

Figure 3.1 Anthropometric dimensions. (a) Trunk Width at the iliac wrest [67], (b) Trunk Length from C7 to L5 [66], (c) Waist Height and Trochanteric height [65]. Adapted from "Human Male And Female Body Line Art", *FreeSVG.org*, https://freesvg.org/1549491622. Accessed 14/August/2020.

Podbevsêk [68] reported the distance between the waist and hip to be approximately 20 cm. On the other hand, the National Aeronautics and Space Administration (NASA) Anthropometry Source Book [65] reported that the distance between the trochanteric height and waist height was approximately 21 cm (shown in Table 3.1). Given these measurements, the total height from L1 to S5 is approximated to be 20 cm for a healthy female of 25 - 40 years old. In this thesis, the sacrum area of the back was excluded to maintain the comfortability by reducing the area covered by the inductive sensor. Additionally, reducing the placement area of the sensor from L1-S5 (20 cm height) to L1-

L5 (10 cm height) provided a flatter surface, which avoided possible wrinkles. Figure 3.2 shows the maximum dimensions of the sensor. These dimensions were used as a reference when designing and evaluating the inductive sensor through the theoretical calculations and simulations.

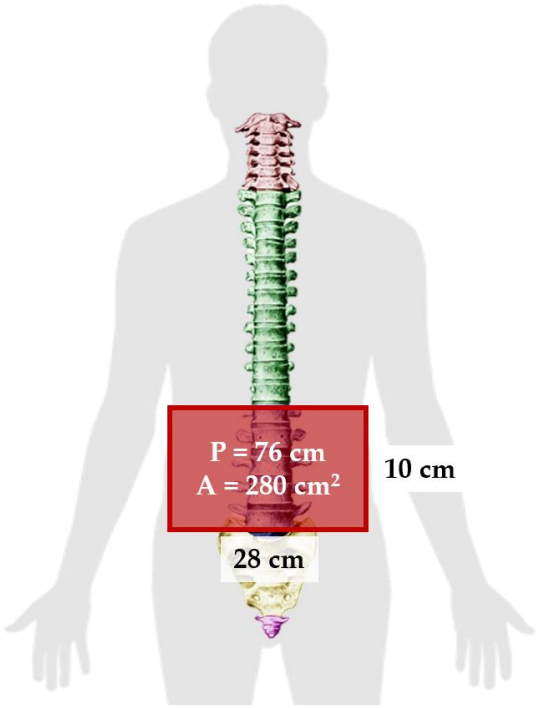

Figure 3.2 Maximum dimensions for the inductive sensor design. P and A represent the perimeter and the area, respectively. These images are licensed under a Creative Commons Attribution-Share Alike license (CC BY -SA). Source images: Columna Vertebras.jpg, *Wikimedia Commons*, https://commons.wikimedia.org/wiki/File:Columna_vertebras.jpg. Accesses on 14/August/2020, CC BY-SA; Human body silhouette.svg, *Wikimedia Commons,* https://commons.wikimedia.org/wiki/File:Human_body_silhouette.svg. Accessed 14/August/2020.

3.3. Theoretical Calculation of the Inductance Value for a Rectangular Sensor

This section presents the theoretical approach used to calculate the inductance of the sensor. In designing the sensor, two approaches were considered: first, the calculation of a simple rectangle based on its dimensions, such as height, width, perimeter, and area [69]–[71]. Second, the calculation of a flat rectangle coil using the Terman equation was performed to evaluate the inductance change when using different number of complete loops [70]. In both approaches, the inductance behavior was analyzed when the height, width, perimeter, area, or number of loops were modified.

3.3.1. Inductance of a Rectangle with Round Wire

Thompson [69] and Grover [71] presented several equations to calculate the inductance based on the shape of an antenna and the type of wire used. The two equations used to calculate the inductance of a rectangle are [69], [71]:

$$L \simeq \frac{\mu_0 p}{2\pi}\left[\ln\left(\frac{2p}{R}\right) + 0.25 - \ln\left(\frac{p^2}{a}\right)\right] \tag{3.1}$$

$$L \simeq \frac{\mu_0 \mu_r}{\pi}\left[-2(W+H) + 2\sqrt{H^2+W^2} - Hln\left(\frac{H+\sqrt{H^2+W^2}}{W}\right) - Wln\left(\frac{W+\sqrt{H^2+W^2}}{H}\right) + Hln\left(\frac{2H}{R}\right) + Wln\left(\frac{2W}{R}\right)\right] \tag{3.2}$$

Where μ_0 is the magnetic permeability of free space equal to $4\pi\times10^{-7}$ H/m and μ_r is the relative permeability of the material inside the rectangle loop. The variable μ_r is considered to be air, the value of which is 1. The perimeter of the polygon is p, the area of the polygon is a, the width of the rectangle is W, the height of the rectangle is H, and finally, the radius of the wire is R.

Equation (3.1) calculates the inductance of a polygon, with any perimeter and area, composed of a round wire. Figure 3.3 shows the inductance behavior based on equation (3.1). From Figure 3.3 it is noticeable that the inductance increases with an almost linear behavior when the area is kept constant and the perimeter increases.

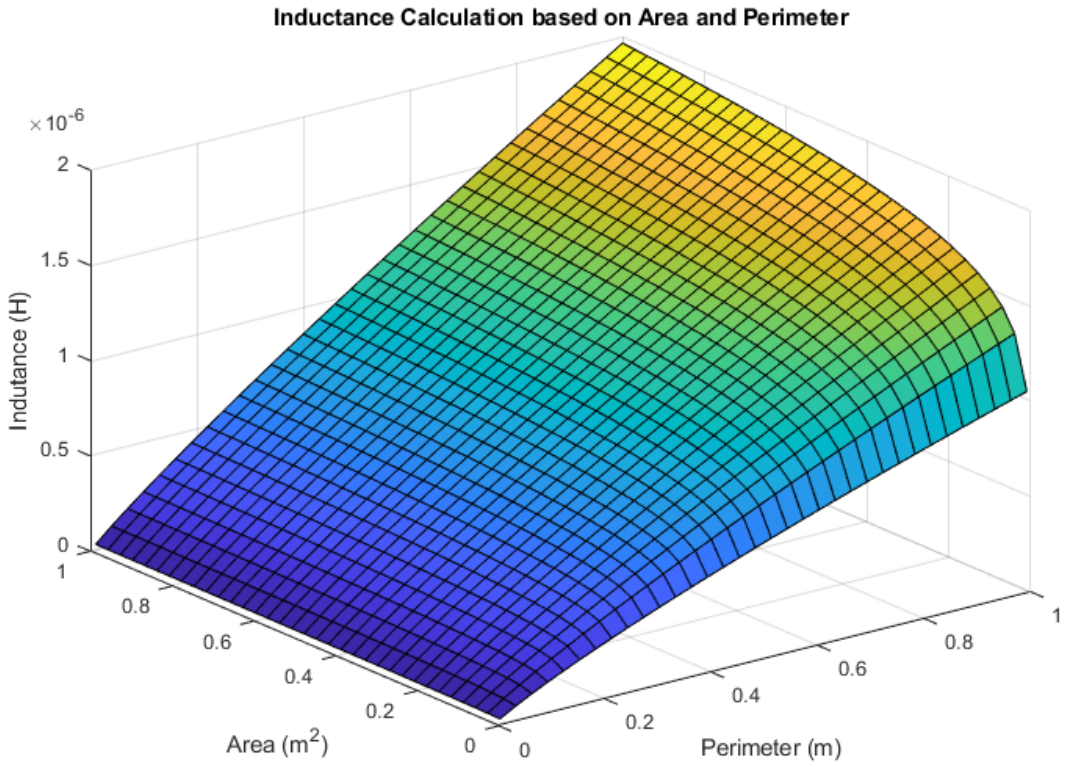

Figure 3.3 Inductance (H) behavior based on the area (m^2) and perimeter (m) of a polygon with round wire.

Equation (3.2) calculates the inductance value according to the height and width of the rectangle loop. Figure 3.4 illustrates the behavior of equation (3.2), where both the height and width are in meters and the inductance is in henries. From Figure 3.4 we can observe that the inductance rapidly increases with a linear behavior when the height is kept constant and the width increases. Equation (3.2) shows a linear behavior regardless of the variable kept constant.

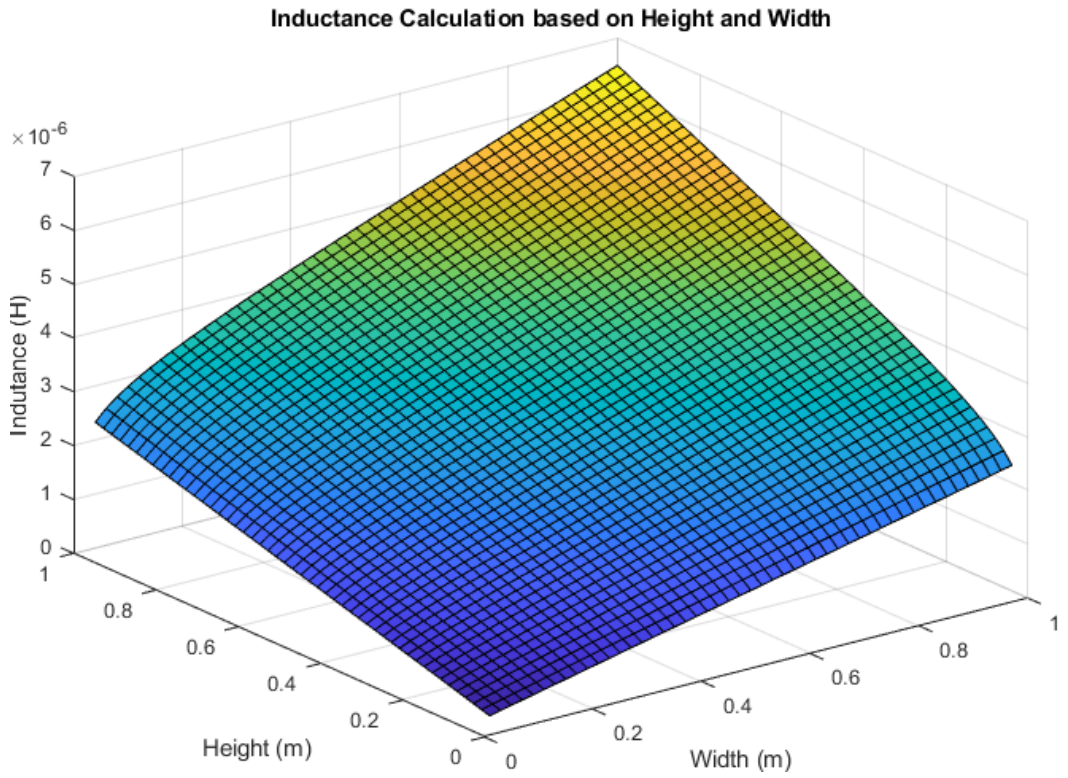

Figure 3.4 Inductance (H) behavior based on the height (m) and width (m) of a rectangle loop.

Additionally, both equations neglect the loop's material but do consider the radius of the wire.

3.3.2. Flat Rectangular Coil

Terman [70] developed equation (3.3) to calculate the low-frequency inductance of a flat rectangular coil. This equation depends on the average dimensions of the rectangle and the number of complete turns of the wire [70]:

$$L \simeq 0.02339n^2\left[(s_1+s_2)log_{10}\frac{2s_1s_2}{nD} - s_1log_{10}(s_1+g) - s_2log_{10}(s_2+g)\right] + 0.01016n^2\left(2g - \frac{s_1+s_2}{2} + 0.447nD\right) - 0.01016n(s_1+s_2)(A+B) \quad (3.3)$$

where s_1 and s_2 are average dimensions of the rectangle, g is the average diagonal $g = \sqrt{{s_1}^2 + {s_2}^2}$, n is the number of complete turns with a pitch of winding D. Figure 3.5 illustrates the flat rectangular coil configuration.

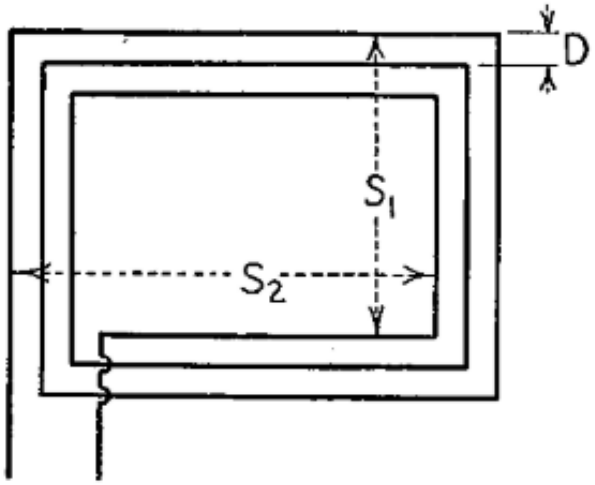

Figure 3.5 Flat rectangle coil geometry presented by Terman [70].

Furthermore, A and B are correction constants based on the wire spacing and the number of turns, respectively. Table 3.2 shows the correction constants A from 0.01 to 0.1 and Table 3.3 shows the B correction constants from 1 to 10. Complete tables for correction constants A and B can be found in the Radio Engineers' Handbook by Terman [70]. Terman used the English system for calculations in equation (3.3), therefore, the dimensions are in inches.

Table 3.2 Correction values of constant A in equation (3.3) from 0.01 to 0.1

Wire diameter/ D (in)	**A**
0.01	-4.048
0.02	-3.355
0.03	-2.950
0.04	-2.662
0.05	-2.439
0.06	-2.256

0.07	-2.102
0.08	-1.969
0.09	-1.851
0.1	-1.746

Table 3.3 Correction values of constant *B* in equation (3.3) from 1 to 10

Number of turns (n)	B
1	0.000
2	0.114
3	0.166
4	0.197
5	0.218
6	0.233
7	0.244
8	0.253
9	0.260
10	0.266

Similar to equation (3.1) and (3.2), equation (3.3) does not consider the material of the sensor. Moreover, the diameter of the wire is only considered in the correction constant *A*. The geometry and symmetry of the sensor in equation (3.3) are extremely important given that average dimensions (s_1, s_2, and g), as well as the distance between loops D, are considered. Therefore, a slight modification in the geometry of the sensor during the manufacturing process can have a great impact on the inductance value.

3.4. Simulating Inductance Value of a Rectangle Using Ansys

A series of simulations were performed in Ansys 2019 R2/19.4 Electromagnetics (Ansys Inc., Canonsburg, Pennsylvania) using Ansys Maxwell 3D design. As mentioned before, the objective of simulations was to verify the theoretical calculations and evaluate the

inductance behavior when variables such as the material of the sensor (copper) and its surrounding (air) are considered. Table 3.4 shows the parameters used in the Ansys simulations for this chapter. Figure 3.6 illustrates the characteristics of the single loop rectangle used for simulations in section 3.4.1 and 3.4.2

Table 3.4 Parameters used for simulating inductance value using Ansys.

Ansys' Parameters		**Sensor**
Sensor's Characteristics	Material	Copper
	Wire Diameter	0.14 mm
Box Characteristics	X	600 mm
	Y	150 mm
	Z	100 mm
	Material	Air
Setup	Maximum # Passes	10
	% Error	1
	% Refinement Per Pass	30
	Minimum # of Passes	5
	Minimum Converged Passes	1
Mesh		Classic, Small
Excitation		1.56 mA

In Table 3.4, "Sensor's Characteristics" describes the properties used in this chapter for all the simulations performed in Ansys. Moreover, Ansys Maxwell 3D requires delimitation of the space, denoted by "Box" in Table 3.4, and to specify the material of the object which in this case was air. The "Setup" parameters are [72]:

1. Maximum Number of Passes defines a limit on the adaptive refined passes that the solver performs.

2. Percentage of Error defines the goal for the Error Energy and Delta Energy.

3. Percentage of Refinement Per Pass determines the number of tetrahedral elements added in the mesh refinement.

4. Minimum Number of Passes defines the minimum number of adaptive passes before the simulation stops.

5. Minimum Converged Passes determines the minimum number of adaptive passes that should converge before the solution stops.

Additionally, "Mesh" is the computer process of redefining an object in a finite number of tetrahedra, and "Excitation" is the current that runs through the sensor.

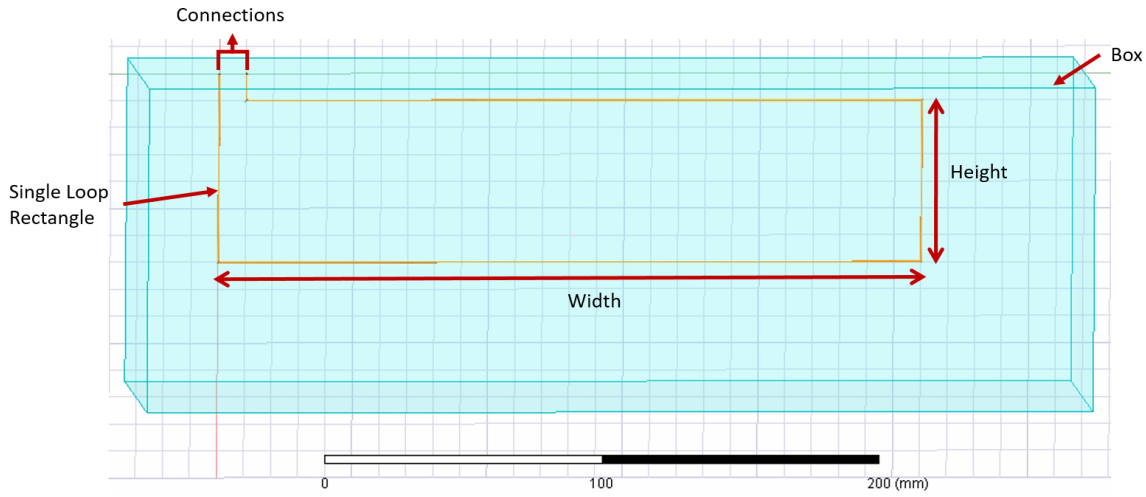

Figure 3.6 Single loop rectangle simulated in Ansys for Section 3.4.1 and Section 3.4.2.

3.4.1. Inductance Change Based on Perimeter and Area

This section explores the effect of changing the perimeter and area of a single loop rectangular sensor on the inductance value. The performed simulations were divided in two sets keeping the area constant in one set and keeping the perimeter constant in the other one. Tables 3.5 and 3.6 show the specifications of the first and second set of simulations, respectively.

Table 3.5 Single loop rectangle dimensions with a constant area (15,600 mm^2).

Perimeter (mm)	Width (mm)	Height (mm)
556	200	78
581.82	220	70.91
610	240	65
640	260	60
671.42	280	55.71
704	300	52
734.5	320	48.75

Table 3.6 Single loop rectangle dimensions with a constant perimeter (640 mm).

Area (mm^2)	Width (mm)	Height (mm)
3 100	310	10
6 000	300	20
11 200	280	40
15 600	260	60
19 200	240	80
22 000	220	100
24 000	200	120
25 200	180	140
25 600	160	160

3.4.2. Inductance Change Based on Height and Width

This section investigates the variations in the inductance of a single loop rectangle with changing the height and width. Similarly to the previous section, simulations were divided in two sets, each maintaining either a constant height or a constant width for the single loop rectangle. Table 3.7 shows the specifications of the first and second sets of simulations.

Table 3.7 Single loop rectangle dimensions with keeping either height or width constant.

Constant Height (60 mm)	Constant Width (260 mm)
Width (mm)	**Height (mm)**
230	30
240	40
250	50
260	60
270	70
280	80
290	90

3.4.3. Inductance Change Based on the Number of Loops in a Flat Rectangular Coil

The relationship between the inductance value and the number of loops in a flat rectangle coil was also investigated. The distance between each loop *D* was arbitrarily set to 10 mm. Figure 3.7 illustrates an example of the flat rectangular coil simulated in Ansys.

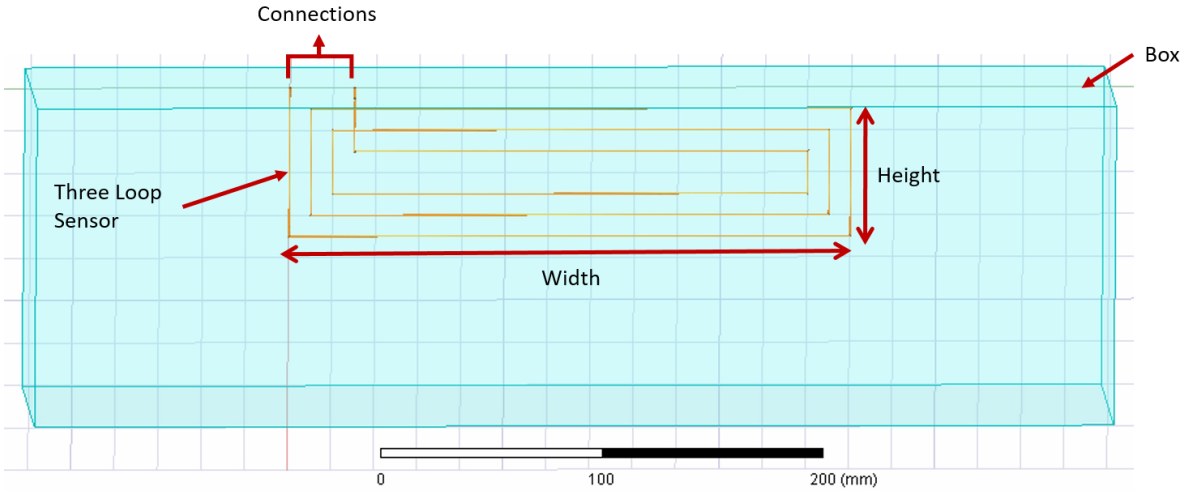

Figure 3.7 Flat rectangular coil with three turns simulated in Ansys.

3.5. Results

This section compares the results obtained from the theoretical calculations in Section 3.3 and the simulations in section 3.4. The data of both sections were processed using MATLAB R2018b (The MathWorks, Inc., Natick, Massachusetts).

3.5.1. Comparison Between Calculations and Simulations: Inductance Change Based on Perimeter and Area

Table 3.8 and Table 3.9 show the results of the calculated inductance from simulations. In Table 3.8 the area is kept constant; while in Table 3.9 the constant parameter is the perimeter.

Table 3.8 Inductance calculation of a single loop rectangle with a constant area (15,600 mm^2) using Ansys simulations and equation (3.1).

Perimeter (mm)	Width (mm)	Height (mm)	Simulation Inductance (nH)	Equation (3.1) Inductance (nH)
556	200	78	731.865	694.28
581.82	220	70.91	762.972	721.24
610	240	65	790.339	750.40
640	260	60	832.576	781.16
671.42	280	55.71	870.783	813.08
704	300	52	901.676	845.86
737.5	320	48.75	941.019	876.27

Table 3.9 Inductance calculation of a single loop rectangle with a constant perimeter (640 mm) using Ansys simulations and equation (3.1).

Area (mm^2)	Width (mm)	Height (mm)	Simulation Inductance (nH)	Equation (3.1) Inductance (nH)
3 100	310	10	680.557	574.33
6 000	300	20	757.299	658.86

11 200	280	40	804.619	738.75
15 600	260	60	832.576	781.16
19 200	240	80	835.797	807.74
22 000	220	100	847.971	825.16
24 000	200	120	840.832	836.30
25 200	180	140	842.452	842.55
25 600	160	160	854.903	844.56

Figure 3.8 and Figure 3.9 illustrate the inductance behavior calculated using equation (3.1) (blue curve) as well as the simulation results (orange curve) when the area is constant, respectively.

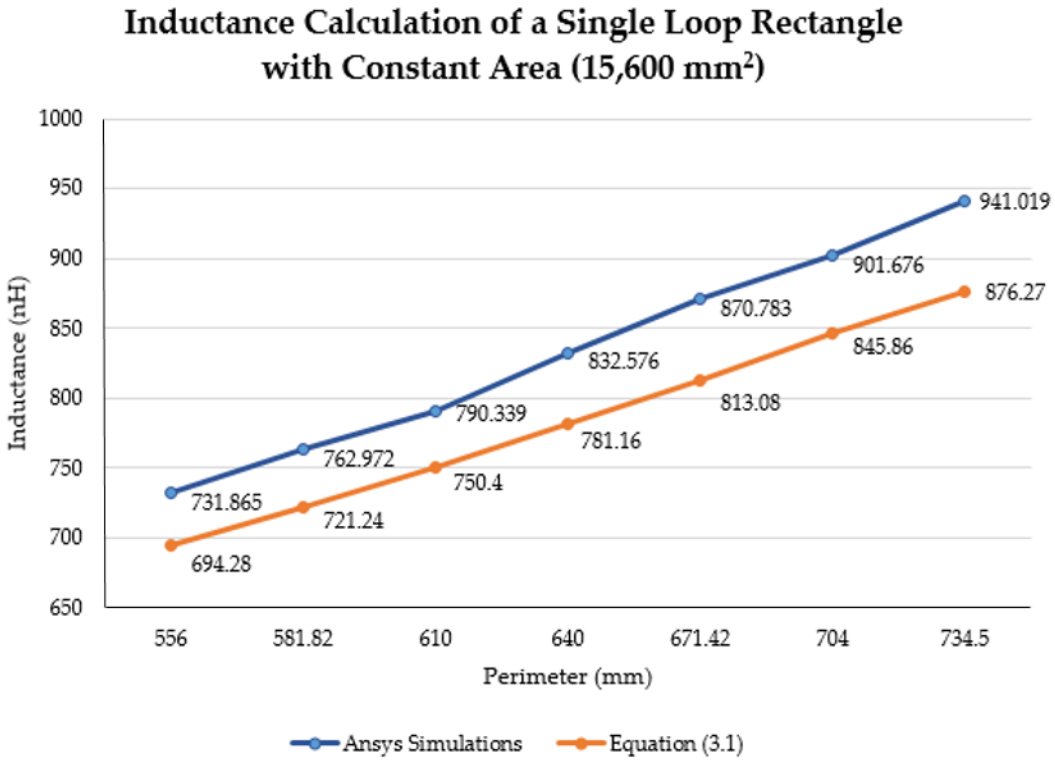

Figure 3.8 Theoretical and simulated inductance calculation (nH) with a constant area (15,600mm²).

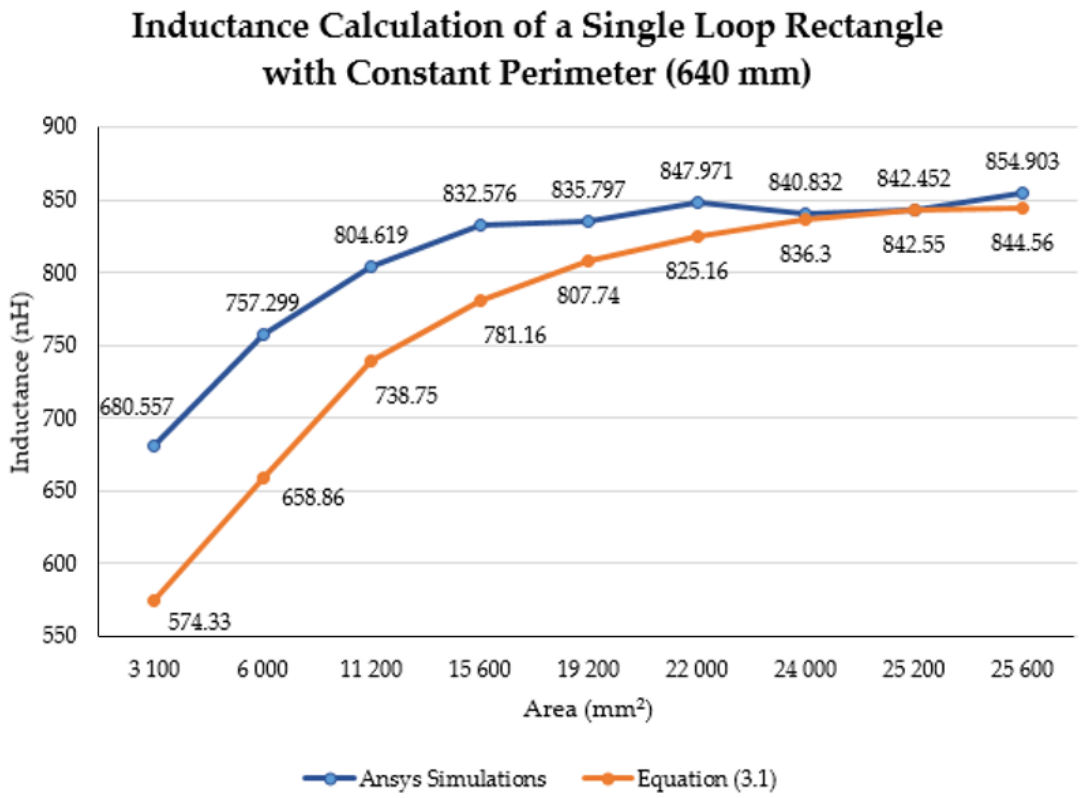

Figure 3.9 Theoretical and simulated inductance calculation (nH) with a constant perimeter (640 mm).

Figure 3.10 and Figure 3.11 show the comparison between simulation results and theoretical calculations. Figure 3.10 presents the inductance values when the area is kept constant. The blue dashed line is the inductance value that resulted from equation (3.1) using a constant area of 15,600 mm^2; while the red line is the inductance calculated using the same equation but using the maximum dimensions of the lumbar area (28,000 mm^2) presented in Section 3.2. Furthermore, the yellow "x" represents the inductance resulting from simulations with a constant area of 15,600 mm^2. The purple line is the MATLAB polynomial curve fitting (polyfit) function using a first-degree polynomial. Finally, the bold grey lines represent the maximum perimeter for the lumbar section of a healthy participant (760 mm).

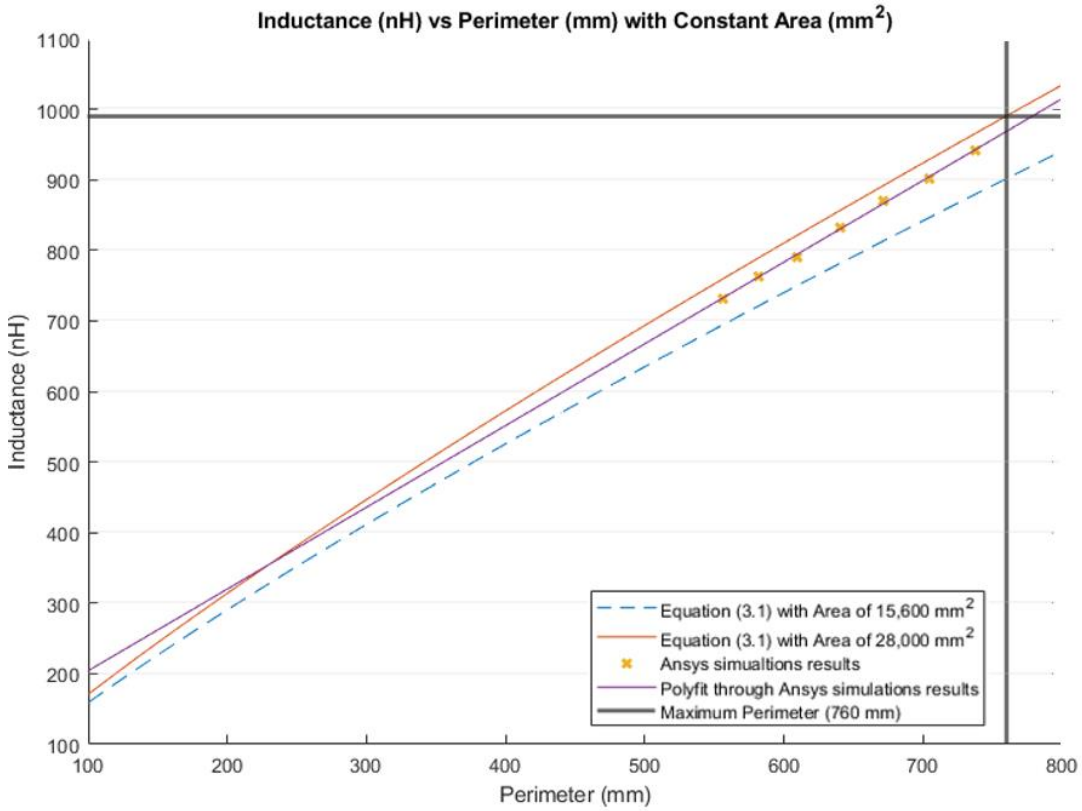

Figure 3.10 Comparison between the theoretical inductance calculations using equation (3.1) with a constant area (mm^2) and simulations results.

Figure 3.11 illustrates the inductance calculations when the perimeter is constant. Similar to Figure 3.10, the blue dashed line represents the inductance calculations using equation (3.1) with a constant perimeter of 640 mm. The inductance obtained using the same equation with the maximum perimeter of the lumbar section (760 mm) is depicted as a red line. Moreover, the yellow "x" represents the inductance obtain by the simulations with a constant perimeter of 640 mm. The purple line is the MATLAB cubic spline data interpolation (spline) function that passes through the simulations results. Finally, the bold grey lines represent the maximum area (28,000 mm^2) for the lumbar section of a healthy participant.

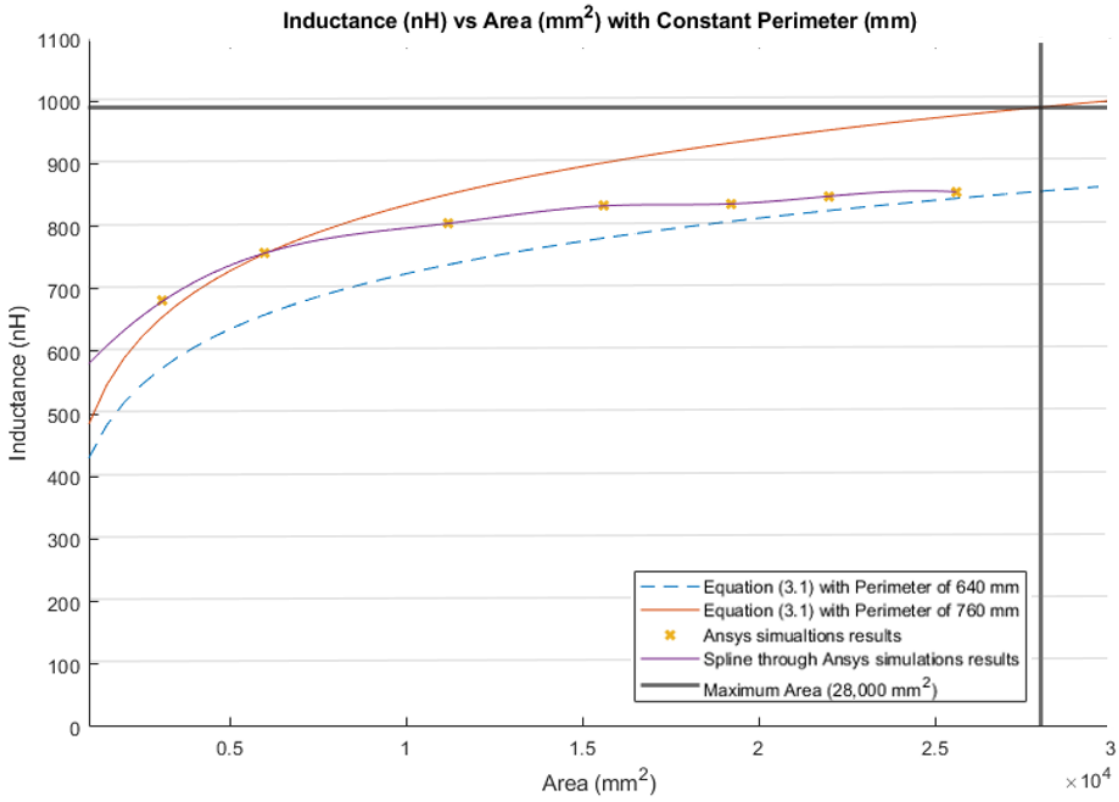

Figure 3.11 Comparison between theoretical inductance calculations using equation (3.1) with a constant perimeter (mm) and simulations results.

The inductance value corresponding to the maximum dimensions of the lumbar area of a healthy female participant (280 mm × 100 mm) using equation (3.1) was calculated to be 990.41 nH.

3.5.2. Comparison Between Calculations and Simulations: Inductance Change Based on Height and Width

Table 3.10 shows the inductance results from simulations when the height was kept constant. Table 3.11 presents the inductance obtained from simulations when the width was held constant.

Table 3.10 Inductance calculation of a single loop rectangle with a constant height (60 mm) using Ansys simulations and equation (3.2).

Width (mm)	Simulations Inductance (nH)	Equation (3.2) Inductance (nH)
230	743.565	670.09
240	769.836	694.39
250	795.330	718.70
260	821.577	742.99
270	846.542	767.29
280	871.462	791.57
290	896.130	815.86

Table 3.11 Inductance calculation of a single loop rectangle with a constant width (260 mm) using Ansys simulations and equation (3.2).

Height (mm)	Simulations Inductance (nH)	Equation (3.2) Inductance (nH)
30	711.167	606.58
40	752.310	657.07
50	788.522	701.79
60	821.577	742.99
70	849.815	781.86
80	874.200	819.08
90	893.009	855.08

The inductance behavior with changing the width and height is shown in Figure 3.12 and Figure 3.13, respectively.

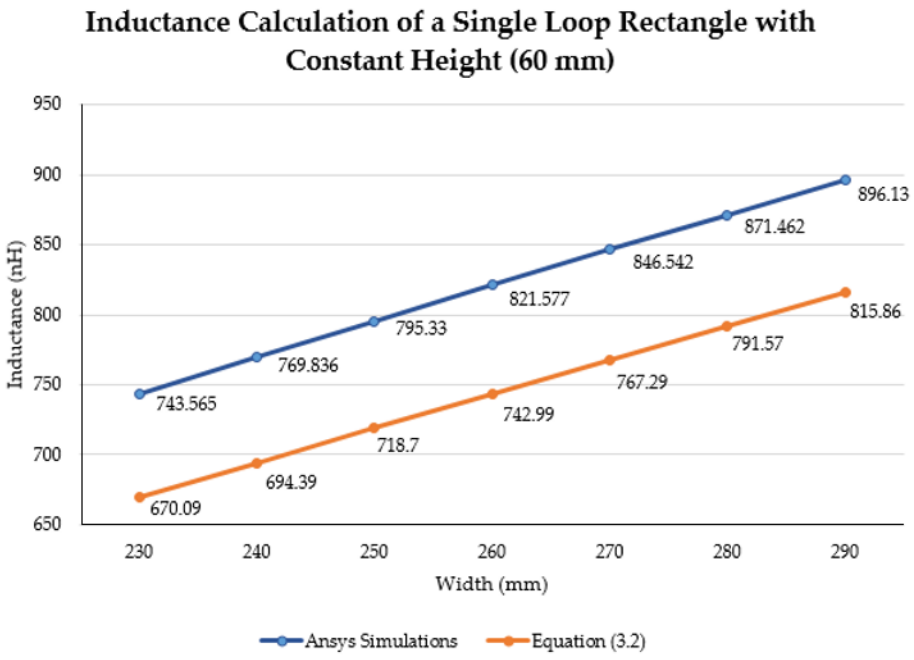

Figure 3.12 Inductance calculation (nH) using equation (3.2) and Ansys simulations with a constant height (60 mm).

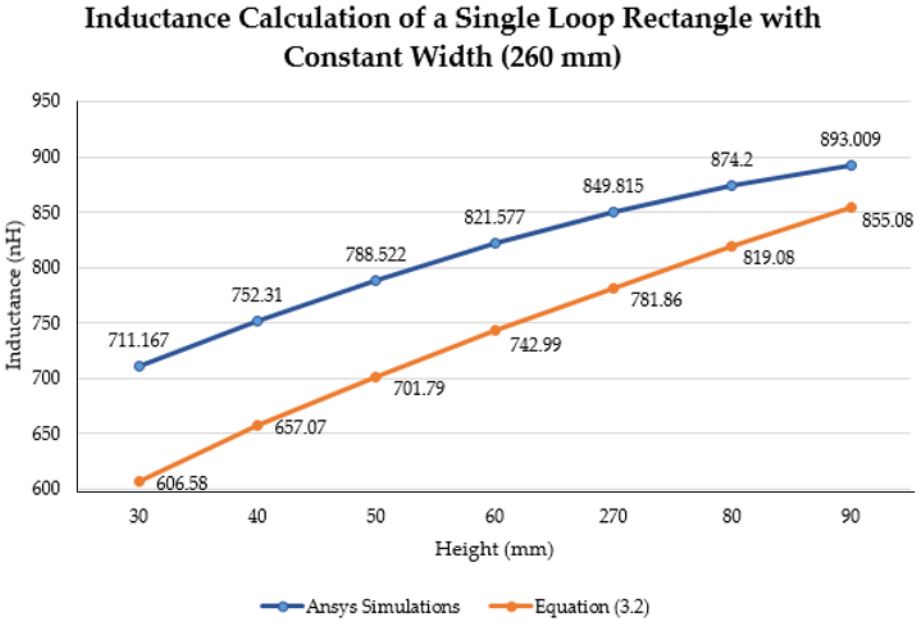

Figure 3.13 Inductance calculation (nH) using equation (3.2) Ansys simulations with a constant width (260 mm).

Figure 3.14 and Figure 3.15 show the comparison between the results of simulations and those of equation (3.2). Figure 3.14 illustrates the inductance values with varying the width and maintaining a constant height. The blue dashed line represents the results from equation (3.2) with a constant height of 60 mm. The red line is the inductance calculated from the same equation, but with a constant height of 100 mm; which is the total height of the lumbar section according to the anthropometrics represented in section 3.2. Additionally, the bold grey lines represent the maximum width for the lumbar section (280 mm). The yellow "x" represents the inductance values simulated with a constant height of 60 mm. Finally, the purple line is the MATLAB polynomial curve fitting (polyfit) function using a first-degree polynomial.

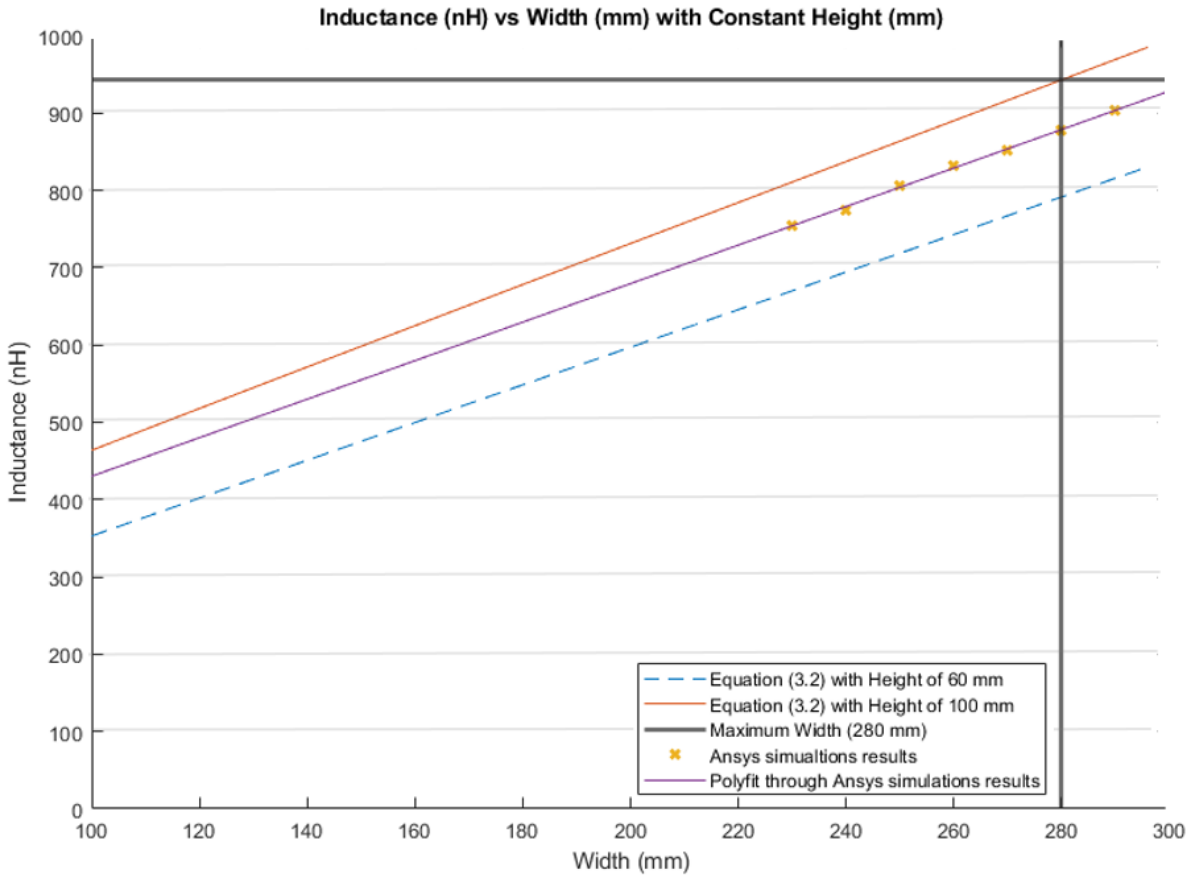

Figure 3.14 Comparison between theoretical inductance calculations using equation (3.2) and simulation results with a constant height (mm).

Figure 3.15 shows the results of calculating the inductance value with a variable height and a constant width using equation (3.2). The blue and red lines represent the inductance results calculated with a constant width of 260 mm and 280 mm, respectively. The bold grey lines represent the maximum lumbar height (100 mm). The yellow "x" markers represent the inductance results from the simulations run using a constant width of 260 mm. Finally, the purple line is the MATLAB cubic spline data interpolation (spline) function based on the simulation results.

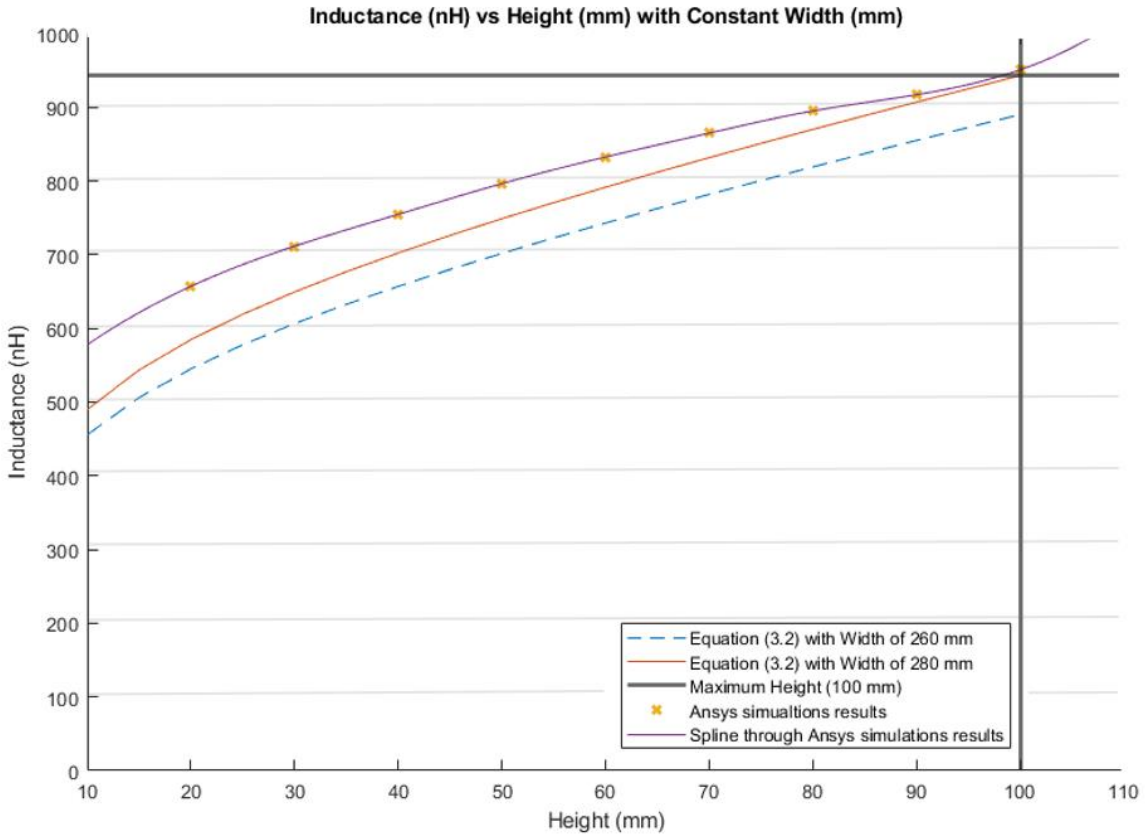

Figure 3.15 Comparison between the theoretical inductance calculations using equation (3.2) and simulation results using a constant width (mm).

The inductance value obtained from the maximum dimensions of the lumbar section (280 mm × 100 mm) using equation (3.2) was 943.01 nH.

3.5.3. Comparison Between Calculations and Simulations: Inductance Change Based on the Number of Loops in a Flat Rectangular Coil

This section presents the change in the inductance value with varying the number of complete loops using equation (3.3). The chosen dimensions for the flat rectangular coil were 60 mm height and 260 mm width. As mentioned in section 3.4.3, the distance between each loop was 10 mm. The maximum number of complete turns able to fit in the rectangle with the aforementioned dimensions was three. MATLAB cubic spline data interpolation (spline) function was used to interpolate the behavior of the results.

Figure 3.16 illustrates the comparison between the theoretical results from equation (3.3) and simulations in which results of equation (3.3) results are denoted with blue "o" markers and simulation results are marked with orange "x". A MATLAB cubic spline data interpolation (spline) function was used to extrapolate the values and generate the corresponding curve for each case.

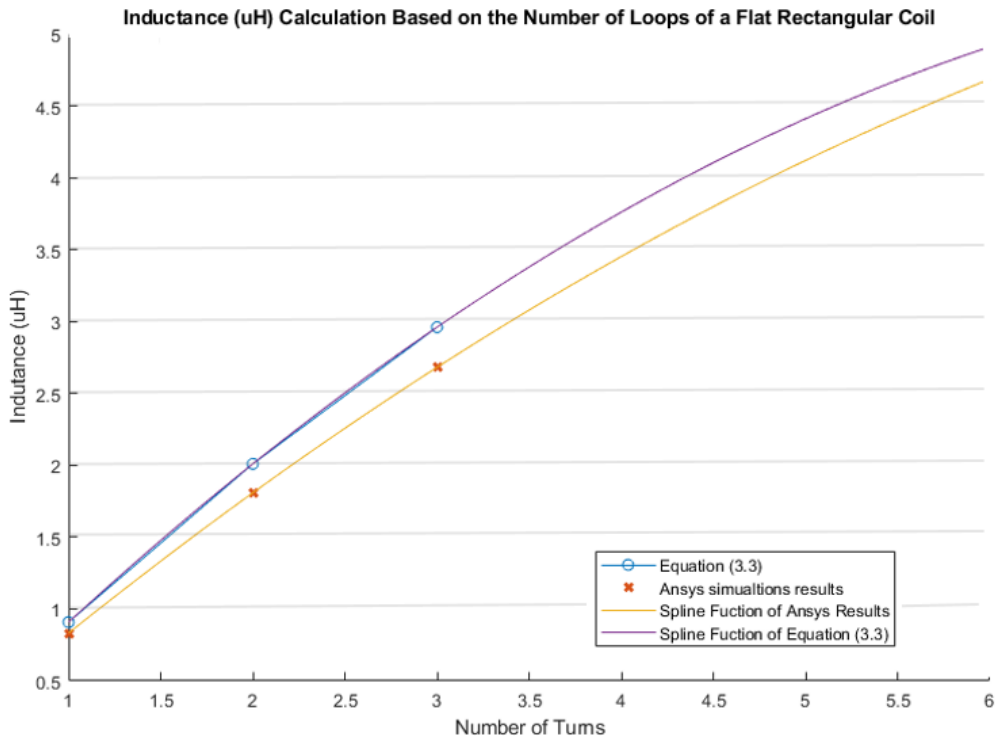

Figure 3.16 Comparison between the results obtained from equation (3.3) and simulations.

3.6. Discussion

The inductance of a single loop rectangle was calculated using two different equations. Figure 3.3 shows the results of equation (3.1); which describes the inductance based on the perimeter and the area. Equation (3.1) demonstrated an almost linear behavior when the area was kept constant. However, in the case of a constant perimeter, the inductance behavior was similar to that of a logarithmic graph. Equation (3.2), which relates the inductance value to the height and width of the rectangle (Figure 3.4), describes the inductance with a linear behavior when the height was constant. On the other hand, when the width was constant, the inductance showed a linear behavior when the height was approximately 25 mm. Unfortunately, these two equations led to different results for the inductance of a single loop rectangle, such that there was a difference of approximately 40 nH between the inductance values calculated using these equations for the same sensor dimensions. This discrepancy in calculated values increased as the rectangle became bigger. An example of this discrepancy can be seen using the lumbar anthropometric dimensions of a healthy participant from section 3.2, where the rectangle had a width of 280 mm and a height of 100 mm. Using equation (3.1), the inductance value was calculated to be 990.42 nH, while using equation (3.2), the inductance was equal to 943.01 nH. The difference between these results was 47.41 nH. The equations used in this chapter are solely based on the geometry of the rectangle loop and entirely neglect the material from which the rectangle loop is made.

Finally, when the inductance was studied based on the height and width rather than the area and perimeter, it was possible to observe a more linear behavior; which facilitates the theoretical prediction of the inductance when using a rectangular shape. The inductance calculation based on the area and perimeter reported had closer results to the simulations compared to the results based on width and height. The average difference between simulation results and equation (3.1) calculations was 49.849 nH and 43.066 nH for constant area and constant perimeter, respectively. The average difference between the simulation results and equation (3.2) calculations was 77.650 nH and 75.164 nH for a

constant height and width, respectively. Additionally, the simulated inductance value using the lumbar anthropometric dimensions was 1.003 μH. The difference between this simulation and the results from equation (3.1) and equation (3.2) using the same lumbar dimensions was 12.58 nH and 59.99 nH, respectively.

In general, the behavior and trend of inductance values were similar in both simulations and theoretical calculations, but the obtained inductance values were different. Nonetheless, the simulations were closer to the results of equation (3.1) compared to those of equation (3.2). All simulations resulted in a higher inductance compared to theoretical calculations. This outcome could be a result of considering the material of the rectangle loop and the environment surrounding the rectangle loop while running the simulations. Furthermore, unlike studies such as [52], [53], the equations presented in this chapter do not consider mutual-inductance or self-inductance. However, inserting these parameters into the calculations increased the complexity.

The dimensions of the inductive textile sensor were chosen based on using the anthropometric dimensions of the lumbar area of a healthy participant and the inductance behavior. A rectangle of smaller dimensions (260 mm width and 60 mm height) was arbitrary selected to compare the inductance value against the maximum inductance for the lumbar section of the back. Based on equation (3.1), this smaller rectangle covered up to 78.81% of the maximum inductance range. While using equation (3.2), the same smaller rectangle covered up to 78.79%. The maximum inductance was obtained by using the dimensions of the entire lumbar section of a healthy participant, and is presented in Section 3.2.

Figure 3.17 and Figure 3.18 show the covered area based on equation (3.1). Moreover, Figure 3.19 and Figure 3.20 illustrate the covered area based on equation (3.2). In both cases, the covered inductance change is highlighted in grey and the black "x" represents the simulation results for a rectangle with dimensions 260 mm × 60 mm.

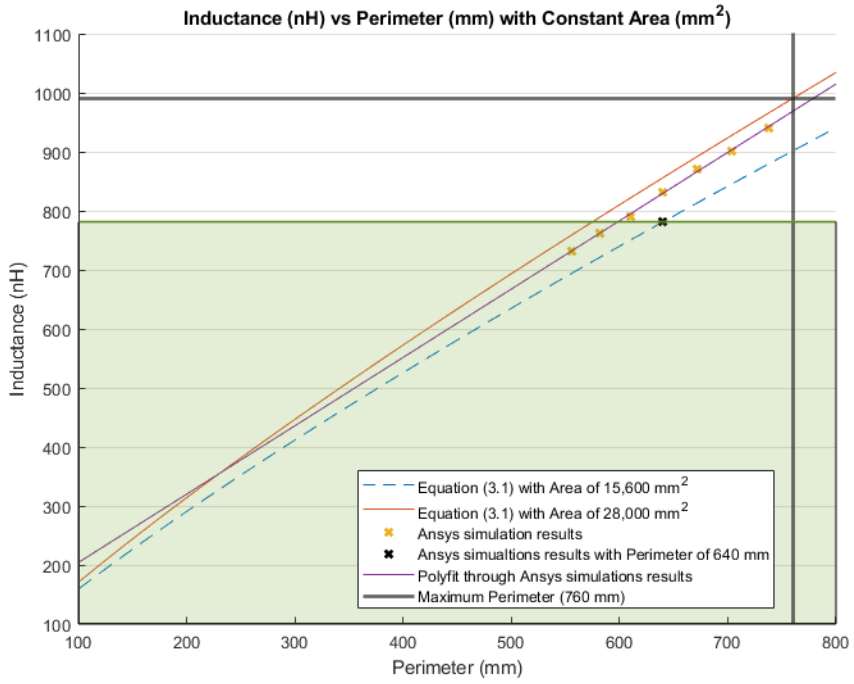

Figure 3.17 Inductance calculation with a constant area (mm²) and a variable perimeter (mm). Highlighted in green shading is 78.81% of the total inductance range.

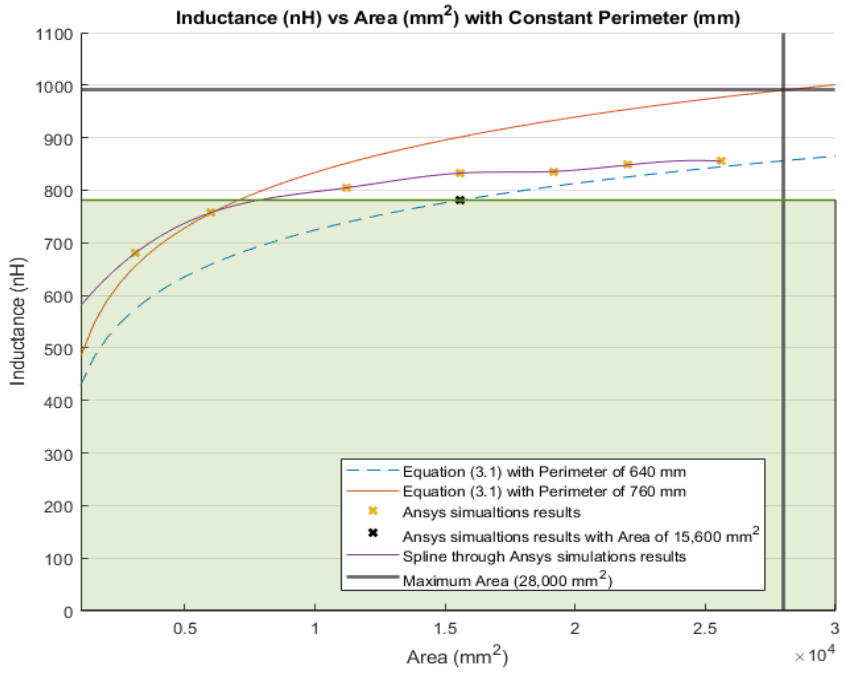

Figure 3.18 Inductance calculation with a constant perimeter (mm) and a variable area (mm²). Highlighted in green shading is 78.81% of the total inductance range.

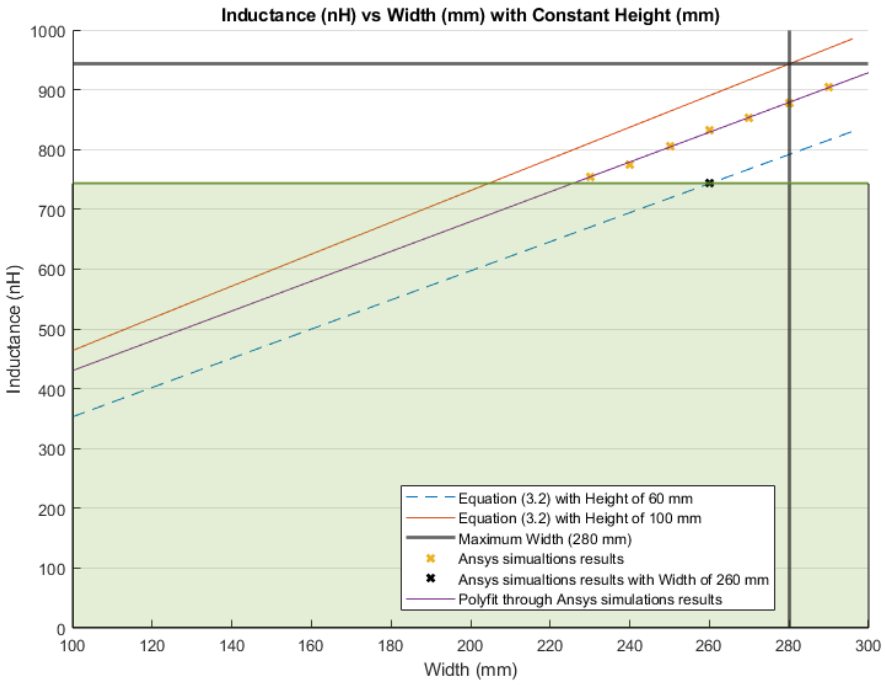

Figure 3.19 Inductance calculation with a constant height (mm) and a variable width (mm). Highlighted in green shading is 78.79% of the total inductance range.

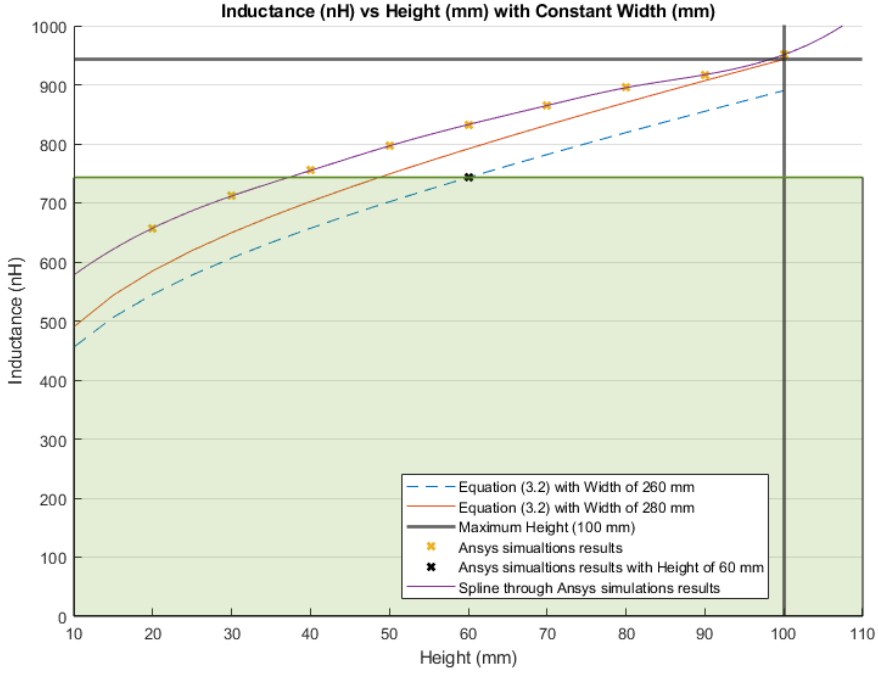

Figure 3.20 Inductance calculation with a constant width (mm) and a variable height (mm). Highlighted in green shading is 78.79% of the total inductance range.

Results of equation (3.3) also differed from those of the simulations. The difference between the inductance value calculated with equation (3.3) and the simulated one increased with the number of loops. More specifically, the inductance value for a single loop was calculated to be 0.909 μH using equation (3.3), while simulations yielded an inductance value of 0.833μH for the same case, resulting in a difference of 0.0759 μH between the two methods. When considering three loops, the difference in the inductance value increased to 0.279 μH, more than twice that obtained for a single loop. Nonetheless, the behavior and trend of inductance were similar using both methods as shown in Figure 3.16.

The percentage reduction of the size and inductance value from the total lumbar dimensions to the arbitrary chosen dimension (260 mm width and 60 mm height) were as follow; the area was reduced to 44.29%, the perimeter was reduced to 15.79%, the height was reduced to 66.67% and finally the width was reduced to 7.14%. These size modifications resulted in a reduction of the inductance by 21.19% and 21.21% for equations (3.1 and 3.2), respectively. Reducing the perimeter and width have a greater impact on the inductance value than on the area and the height. As shown in Figure 3.18 and 3.20, the inductance behavior, when modifying the area and height, followed the pattern of a logarithm. Therefore, when deciding the size of the sensor it was better to modify the area or height to avoid a drastic decrease on its inductance. Additionally, increasing the number of complete loops without modifying the area increased the inductance value.

A rectangle of 260 mm width and 60 mm height proved to cover up to 78.8% of the maximum possible inductance value using both equations (3.1 and 3.2), and consequently, was suggested to be an optimal option when choosing the size of the inductive textile sensor. The maximum number of loops that can be fitted into the aforementioned dimensions was three. Considering that the sensor was made of non-stretchable material, increasing the number of loops will inevitably increase the stiffness of the fabric, which could interfere with the comfort for the user. Among important requirements for wearable

devices are comfort and as unobstructive as possible, so users can perform their normal activities [31], [35], [40], [54].

3.7. Summary

In this chapter, the design of the inductive textile sensor was investigated; first by defining the anthropometric dimension of the lumbar section of a healthy participant and then by studying the inductance behavior using theoretical calculations and extensive simulations.

The theoretical inductance calculation of a single loop rectangle was explored using two different equations. Equation (3.1), related the inductance value to the perimeter and area, while equation (3.2) based its calculation on the width and height of a single loop rectangle. Additionally, the changes of the inductance with varying the number of loops in a flat rectangular coil were analyzed using equation (3.3).

The simulation study was carried out to evaluate the theoretical results from equations (3.1) and (3.2) and highlighted several discrepancies between the results obtained from equations and the simulations. The size of the inductive textile sensor was selected based on two parameters: 1) the anthropometry dimensions of the lumbar section of a healthy participant, and 2) the inductance behavior explored in the theoretical and simulation results. Finally, the adequate number of loops was decided based on the size of the inductive sensor.

Chapter 4

Wearable Device to Monitor Back Movements Using an Inductive Textile Sensor

The material of this chapter is excerpted, modified, and reproduce with permission from the following paper that I co-authored:

- García Patiño, M. Khoshnam, C. Menon. "Wearable Device to Monitor Back Movements Using an Inductive Textile Sensor". Sensors, vol. 20, no. 3, p. 905, 2020.

Sections of this chapter have been adapted from the above paper to fit the scope and formatting of the thesis.

4.1. Introduction

In this chapter, the development of a wireless, comfortable, and compact textile-based wearable platform to track trunk movements when the user bends forward was investigated. The smart garment developed for this purpose was prototyped with an inductive sensor formed by sewing a copper wire into an elastic fabric using a zigzag pattern. The results of an extensive simulation study showed that this unique design increased the inductance value of the sensor, and, consequently, improved its resolution. An experimental evaluation with a healthy participant confirmed that the proposed wearable system with the suggested sensor design detected forward bending movements. The evaluation scenario was then extended to also include twisting and lateral bending of the trunk, and it was observed that the proposed design can successfully discriminate such movements from forward bending of the trunk. Results of the magnetic interference test showed, most notably, that moving a cellphone towards the unworn prototype affects

the sensor readings, however, manipulating a cellphone, when wearing the prototype, did not affect the capability of the sensor to detect forward bends. The proposed platform is a promising step toward developing wearable systems to monitor back posture to prevent or treat LBP.

4.2. Sensor Design and Validation through Simulation

4.2.1. Configuration of the Inductive Textile Sensor

As discussed before, the focus of this study was to detect forward bending of the trunk and discriminate it from other movements such as lateral bending or twisting. The design of the inductive textile sensor was explored and decided in chapter 3. The dimensions chosen for the inductive sensor were 26 cm width and 6 cm height with three complete loops. As presented in the previous chapter, reducing the height and area of the sensor has a smaller impact in the inductance value. Furthermore, increasing the number of loops in the same area increase the inductance value. The inductive sensor in this chapter was created by arranging a copper wire in a zigzag pattern to form an inverted "T" shape, where the horizontal area of the inverted "T" was positioned on the lumbar section of the back to capture strain variations due to forward bend movements. The vertical part of the sensor was used as a framework to align the shirt with the spine. Apart from helping with alignment, the vertical part of the sensor had practical implications; placing the circuitry on the upper area of the back was more practical since the circuitry box caused less discomfort to the user. Furthermore, the vertical part of the sensor allowed for convenient connection of the circuitry to avoid loose cables.

Sewing the sensor into the elastic fabric in a zigzag pattern allowed the fabric to stretch without causing damage or breakage to the sensor. This is an important feature which improves the reliability of the system. Moreover, considering that the length of the wire affects the resulting electrical inductance, the proposed zigzag pattern increased inductance and, thus, improved sensor sensitivity as well as its resistance to interference

from other electrical devices [52]. The dimensions of the zigzag pattern, more specifically its length, angle, and width, were also determining factors in the resulting inductance [73].

4.2.2. Zigzag Pattern

The width of the zigzag pattern was chosen such that the fabric could be sufficiently stretched to accommodate full forward bending without breaking the sensor and affecting the resulting inductance value. To achieve this, a series of Ansys simulations were performed to calculate the change on the inductance value based only on the width of the zigzag. Subsequently, the three simulated sensors with higher inductance values were selected for the next step, which included an experimental evaluation. In this scenario, each sensor was manually stretched up to 200% of its original length to assess its resistance against breakage. The physical inductive sensors were made as similar as possible to the simulation results.

The parameters used in the Ansys simulations and the zigzag parameters are reported in Table 4.1. Figure 4.1a illustrates the characteristics of a single loop inductive sensor and the corresponding Ansys parameters. All parameters of the Ansys simulations were kept constant except for the zigzag width. Figure 4.1b illustrates how the zigzag characteristics were defined.

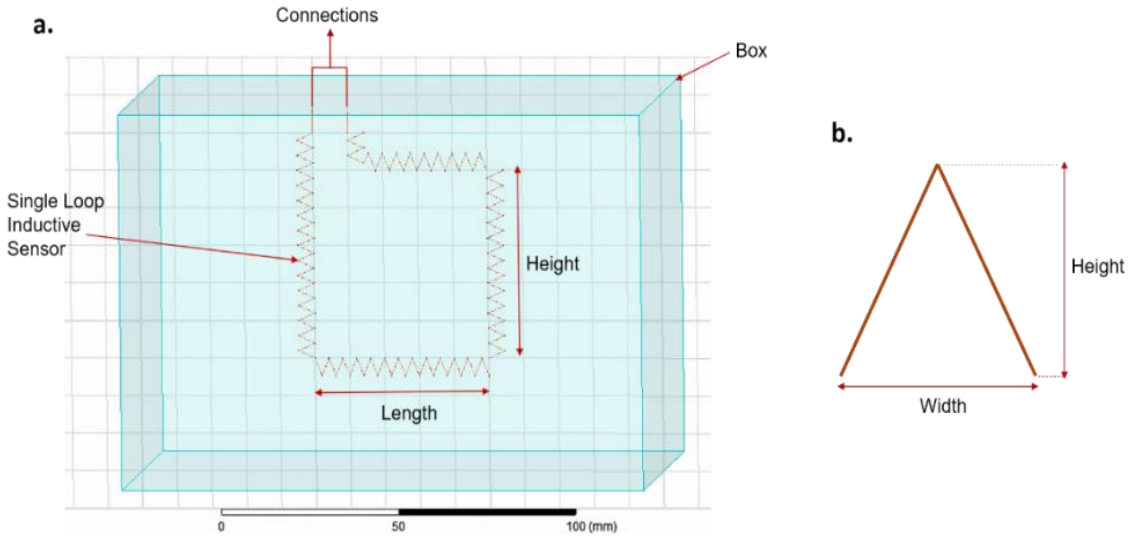

Figure 4.1 Zigzag pattern evaluation in Ansys. (a) Single loop inductive textile sensor; (b) definition of zigzag characteristics. This image is licensed under a Creative Commons Attribution license (CC BY). Source image: A. G. Patiño, M. Khoshnam, and C. Menon, "Wearable device to monitor back movements using an inductive textile sensor," *Sensors (Switzerland)*, vol. 20, no. 3, pp. 5–8, 2020. Avaliable online: https://www.mdpi.com/1424-8220/20/3/905. Accesses on 14/August/2020.

Table 4.1 Parameters and zigzag characteristics used to simulate five single-loop inductive textile sensors in Ansys. Values appearing between dashed lines indicate that the same value was used in all simulations. This table is licensed under a Creative Commons Attribution license (CC BY). Source image: A. G. Patiño, M. Khoshnam, and C. Menon, "Wearable device to monitor back movements using an inductive textile sensor," *Sensors (Switzerland)*, vol. 20, no. 3, pp. 5–8, 2020. Avaliable online: https://www.mdpi.com/1424-8220/20/3/905. Accesses on 14/August/2020.

Ansys' Parameters		**Sensor 1**	**Sensor 2**	**Sensor 3**	**Sensor 4**	**Sensor 5**
Sensors Characteristics	Between Connections	---- 10 mm ----				
	Total Height	---- 60 mm ----				
	Total Length	---- 50 mm ----				
	Material	---- Copper ----				
	Wire Diameter	---- 0.14 mm ----				
Box Characteristics	X	---- 100 mm ----				
	Y	---- 150 mm ----				
	Z	---- 100 mm ----				
	Material	---- Air ----				
Setup	Maximum # Passes	---- 10 ----				
	% Error	----- 5 -----				
	% Refinement Per Pass	---- 30 ----				
	Minimum # of Passes	----- 5 -----				
	Minimum Converged Passes	----- 1 -----				
Mesh		---- Classic, Small ----				
Excitation		---- 1.56 mA ----				
Zigzag Dimensions	Width	2 mm	4 mm	6 mm	8 mm	10 mm
	Height	---- 4.58 mm ----				

The resulting inductance values of the 5 single-loop sensors are shown in Figure 4.2. It was observed that for the same height, the inductance increased when the width of the zigzag decreased. The highest inductance value achieved with a single loop configuration was 532.153 nH at a width of 2 mm, while the lowest value of inductance of 331.711 nH was achieved with a zigzag width of 10 mm.

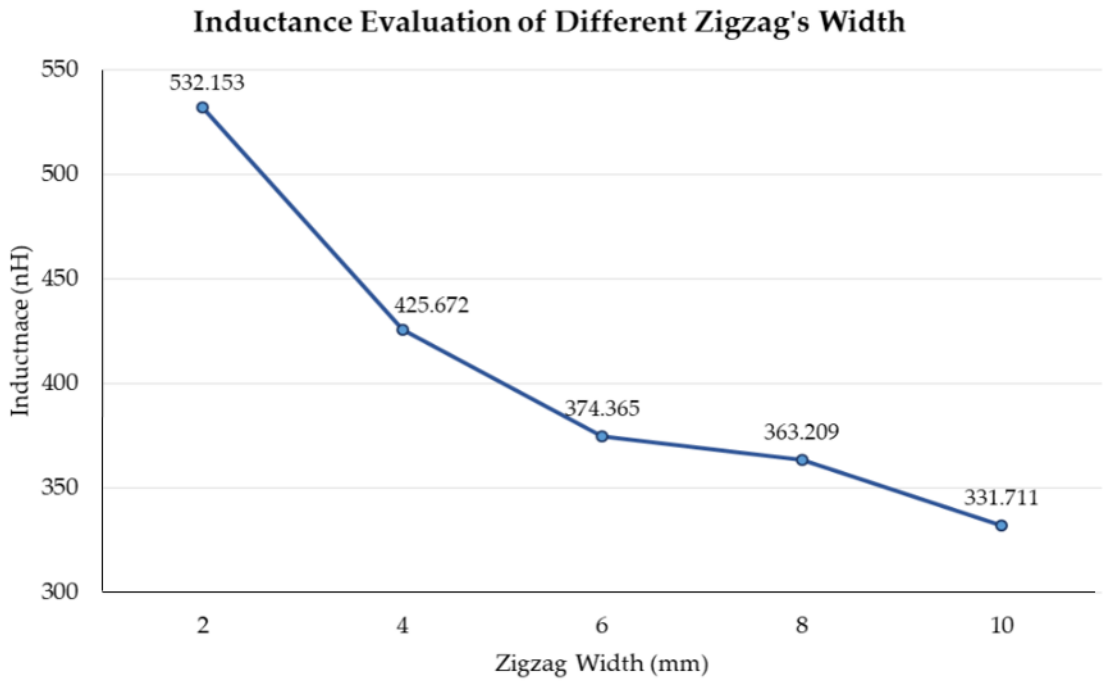

Figure 4.2 Inductance vs zigzag width. Inductance values simulated in Ansys for a single-loop inductive sensor with changing the zigzag width. This image is licensed under a Creative Commons Attribution license (CC BY). Source image: A. G. Patiño, M. Khoshnam, and C. Menon, "Wearable device to monitor back movements using an inductive textile sensor," *Sensors (Switzerland)*, vol. 20, no. 3, pp. 5–8, 2020. Avaliable online: https://www.mdpi.com/1424-8220/20/3/905. Accesses on 14/August/2020.

In the next step, three single-loop inductive sensors with a zigzag width of 2, 4, and 6 mm corresponding to the highest obtained inductance values, 532.153, 425.672, and 347.365 nH, respectively, were constructed. Each inductive sensor was manually stretched up to 200% of its original length. The inductive sensors with zigzag widths of 2 and 4 mm were

successfully stretched without breaking; however, the sensor with the 6 mm zigzag width broke during the stretch.

In terms of functionality and according to the obtained inductance values, sensors generated with 2 and 4 mm of zigzag width exhibited good performance. In terms of comfortability, having a smaller zigzag width increased the stiffness of the fabric and its weight, which potentially interfered with comfort of the user. Therefore, the zigzag with a 4 mm width was chosen due to its high inductance value and its ability to be stretched up to 200% of its original length.

4.2.3. Simulation Study

A simulation study was performed in Ansys 17.2 Electromagnetics Suite (Ansys Inc., Canonsburg, Pennsylvania) to evaluate the design concept proposed in the previous section. In this regard, the effect of the zigzag pattern on electrical inductance and the behavior of the magnetic field of the sensor was investigated. It should be noted that although trunk movements stretch the fabric in all three dimensions only two-dimensional (2D) stretches were considered to reduce the complexity of equations and the computational time. This avoided overloading the computer memory in the simulation phase.

To ensure that the parameters used in simulations were close to the actual corresponding values, 11 reflective markers with a diameter of 8 mm were affixed to the selected piece of garment (a tight-fitting leotard as will be explained in Section 4.3.1) around the section designated for sewing the sensor, as shown in Figure 4.3. A participant was instructed to wear the garment, stand in an upright position, and then bend forward as much as possible without flexing the knees. The position of optical markers during this move was recorded using a Vicon Motion Capture system (Vicon, Oxford, United Kingdom). Collected data were then analyzed in MATLAB R2017b (The MathWorks, Inc., Natick, Massachusetts) to measure the distance between each set of two reflective markers.

Calculated distance values were used in the simulation to represent the dimension of sensors in their original as well as stretched condition. During this test performed in full forward bending position, the garment fabric was stretched to 104% and 132% of its original length in the horizontal and vertical direction, respectively. Therefore, the same stretch values were used in the simulation study.

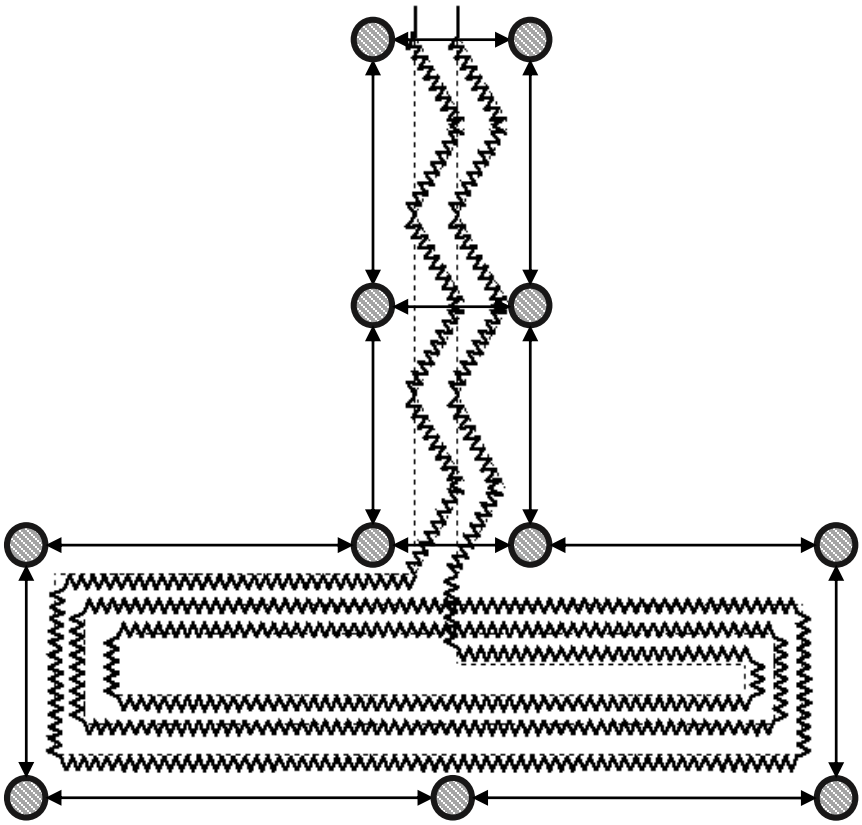

Figure 4.3 Placement of optical markers around the proposed shape for the inductive sensor. Markers are shown as grey circles. This image is licensed under a Creative Commons Attribution license (CC BY). Source image: A. G. Patiño, M. Khoshnam, and C. Menon, "Wearable device to monitor back movements using an inductive textile sensor," *Sensors (Switzerland)*, vol. 20, no. 3, pp. 5–8, 2020. Avaliable online: https://www.mdpi.com/1424-8220/20/3/905. Accesses on 14/August/2020.

To facilitate changing parameter values during the simulation, such as sweep definitions in optometrics, the sensor geometry was built in Ansys Workstation V2.0, and its behavior

was simulated in Ansys Maxwell 3D design. The parameters used to simulate the resulting inductive sensor are shown in Table 4.2. Figure 4.4 illustrates the dimensions of the box and the inductive sensor used in Ansys simulations.

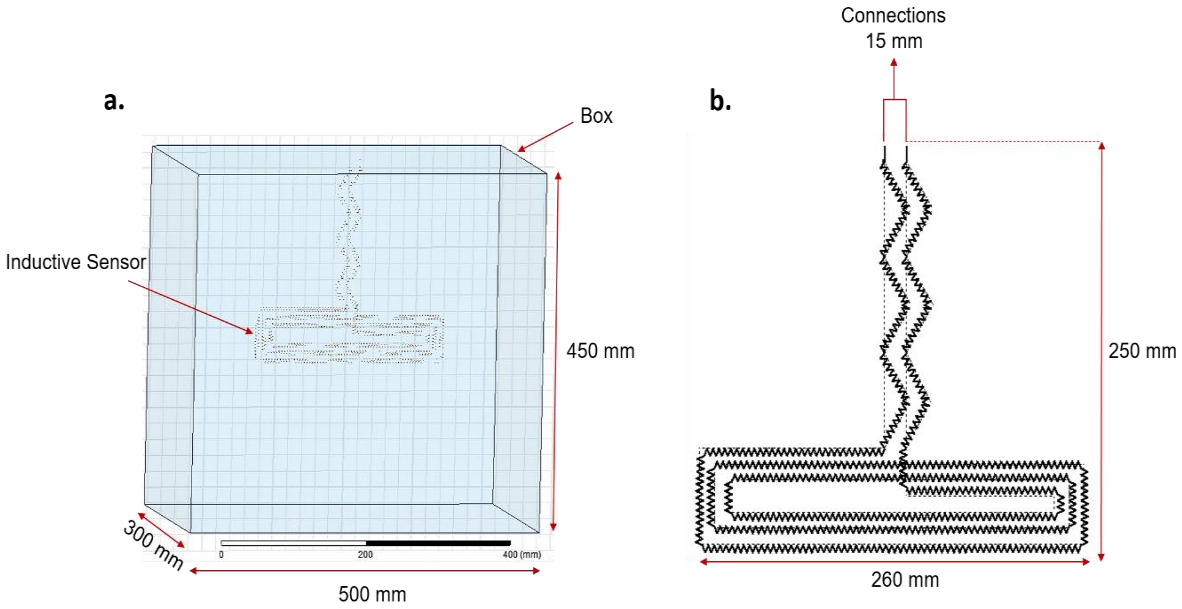

Figure 4.4 Ansys simulation of the inductive sensor: dimensions of the (a) box, (b) inductive sensor. This image is licensed under a Creative Commons Attribution license (CC BY). Source image: A. G. Patiño, M. Khoshnam, and C. Menon, "Wearable device to monitor back movements using an inductive textile sensor," *Sensors (Switzerland)*, vol. 20, no. 3, pp. 5–8, 2020. Avaliable online: https://www.mdpi.com/1424-8220/20/3/905. Accesses on 14/August/2020.

Table 4.2. Parameters used to simulate sensor behavior in Ansys. This table is licensed under a Creative Commons Attribution license (CC BY). Source image: A. G. Patiño, M. Khoshnam, and C. Menon, "Wearable device to monitor back movements using an inductive textile sensor," *Sensors (Switzerland)*, vol. 20, no. 3, pp. 5–8, 2020. Avaliable online: https://www.mdpi.com/1424-8220/20/3/905. Accesses on 14/August/2020.

Inductive Textile Sensor Simulation		
Sensor Characteristics	Distance Between Connections	15 mm
	Total Height	250 mm

	Total Length	260 mm
	Material	Copper
	Wire Diameter	0.14 mm
Box Characteristics	X	500 mm
	Y	450 mm
	Z	300 mm
	Material	Air
Setup	Maximum # Passes	10
	% Error	5
	% Refinement Per Pass	30
	Minimum # of Passes	5
	Minimum Converged Passes	1
Mesh	Classic, small	--
Excitation	--	1.56 mA

In Table 4.2, "Sensor characteristics" correspond to the properties of the inductive textile sensor embedded in the textile. The parameter "Between connections" defines the distance between the two ends of the inductive sensor.

Simulation results showed that with the proposed sensor configuration, the inductance increased from 4.698 μH in an unstretched condition to 5.11 μH in a maximum stretch; which was equivalent to an 8.8% increase in the inductance value. To investigate the effect of the zigzag pattern, the simulation was repeated considering an unstretched sensor without the zigzag pattern. Results indicated that the inductance value, in this case, was 3.476 μH. Comparing this value with that obtained for the unstretched sensor with a zigzag pattern, i.e., 4.698 μH, indicated that the zigzag pattern increased the inductance value by 35%; which pointed to the effectiveness of the proposed configuration in increasing the sensitivity of the sensor.

To observe the electromagnetic field created by the sensor with the proposed geometry and configuration, another simulation study was undertaken using parameters in Table

4.2. The resulting simulated Magnetic Field B (tesla) is shown in Figure 4.5, where the red color represents the highest value and blue represents the lowest value. It was observed that with the proposed sensor design, the magnetic field was stronger around the horizontal section of the inverted "T", which was placed on the lumbar section of the back. This area of higher magnetic field was where the sensor was more sensitive, i.e., a small strain noticeably changed the inductance value. Therefore, such a sensor was well-suited for monitoring forward bending of the trunk (Section 4.2.1).

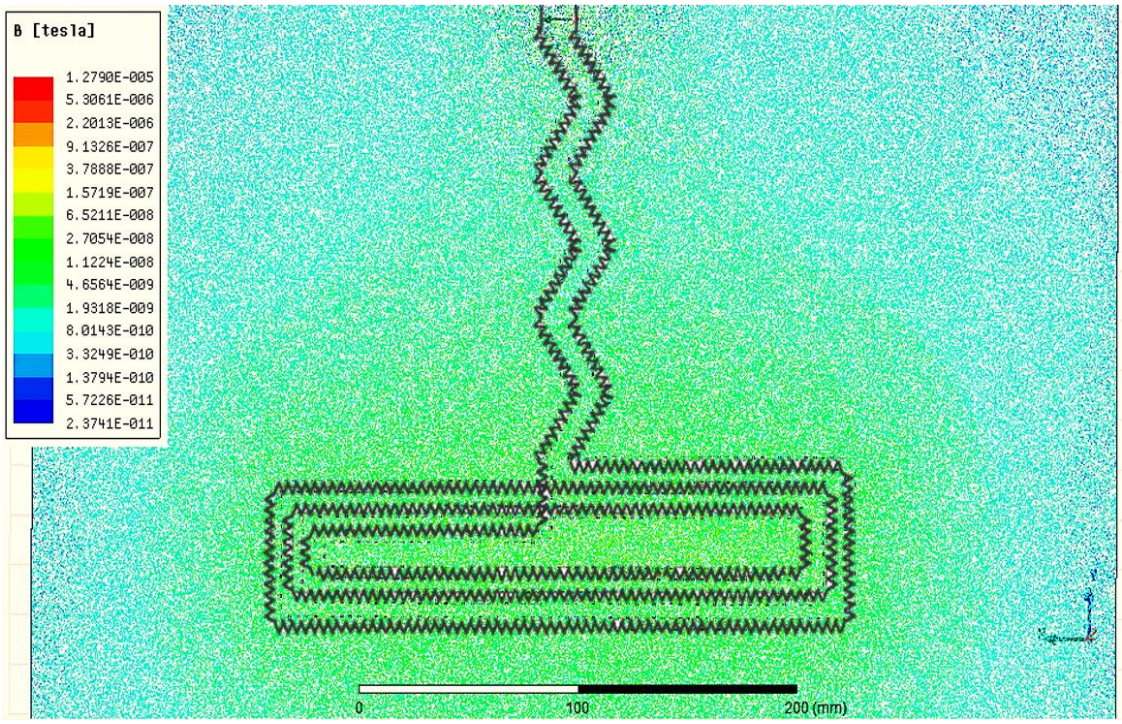

Figure 4.5 Simulation of the electromagnetic field created by the sensor. This image is licensed under a Creative Commons Attribution license (CC BY). Source image: A. G. Patiño, M. Khoshnam, and C. Menon, "Wearable device to monitor back movements using an inductive textile sensor," *Sensors (Switzerland)*, vol. 20, no. 3, pp. 5–8, 2020. Avaliable online: https://www.mdpi.com/1424-8220/20/3/905. Accesses on 14/August/2020.

4.3. Sensor Prototype and Evaluation Protocol

4.3.1. Smart Garment Prototype

To develop the wearable back monitoring platform for this thesis, the inductive textile sensor prototype was integrated within a leotard, which was chosen for its comfort, tightness, and stretching properties. Such a garment can be comfortably worn under a uniform, thus allowing the user to move freely without interfering with their performance of activities of daily living.

To form the inductive sensor, a single copper wire with a diameter of 0.14 mm was sewn into a piece of elastic fabric in the discussed inverted "T" shape using a zigzag stitch (Section 4.2.1) as shown in Figure 4.6. A stabilizer fabric was used to facilitate the sewing process (Figure 4.6b), which later was completely removed. The sewing machine used in this thesis was a PFAFF model Quilt Ambition 2.0. The setup of the sewing machine included a thread tension of 4, three-step zigzag stitch with width of 4, and length of 7 (Figure 4.6c). The elastic fabric with the embedded inductive sensor was then affixed to the back of the leotard such that the vertical part of the inverted "T" was aligned with the spine and the horizontal part was placed on top of the lumbar section of the back as shown in Figure 4.7. The horizontal section of the inverted "T" was a flat coil with 3 concentric loops in a rectangular shape that were separated from each other by 1 cm. During the fabrication process, the inductance values were measured with a pair of smart tweezers (LCR Pro1, LCR Research, Toronto, Ontario, Canada) at a frequency of 100 Hz.

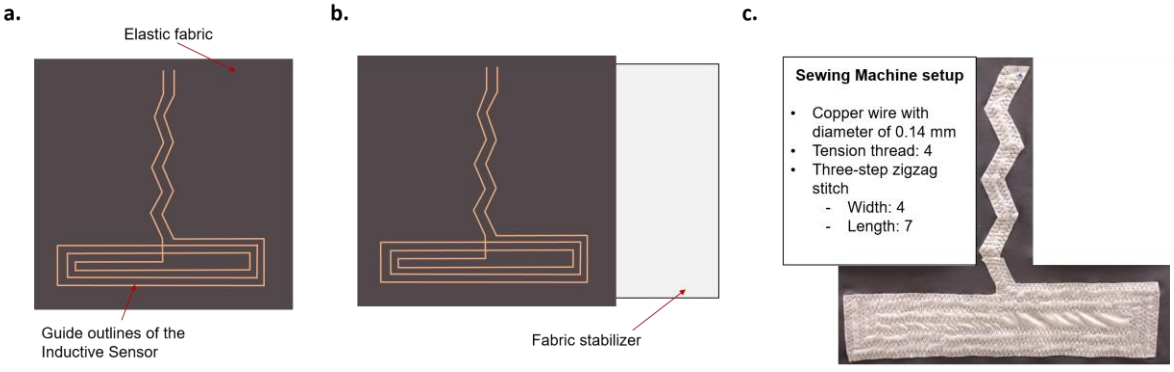

Figure 4.6 Sewing process for the inductive textile sensor. (a) guide outlines are drawn in the elastic fabric to later sew on top of them; (b) a fabric stabilizer is positioned under the elastic fabric to facilitate the sewing process; (c) sewing machine setup and illustration of the inductive sensor with stabilizer fabric.

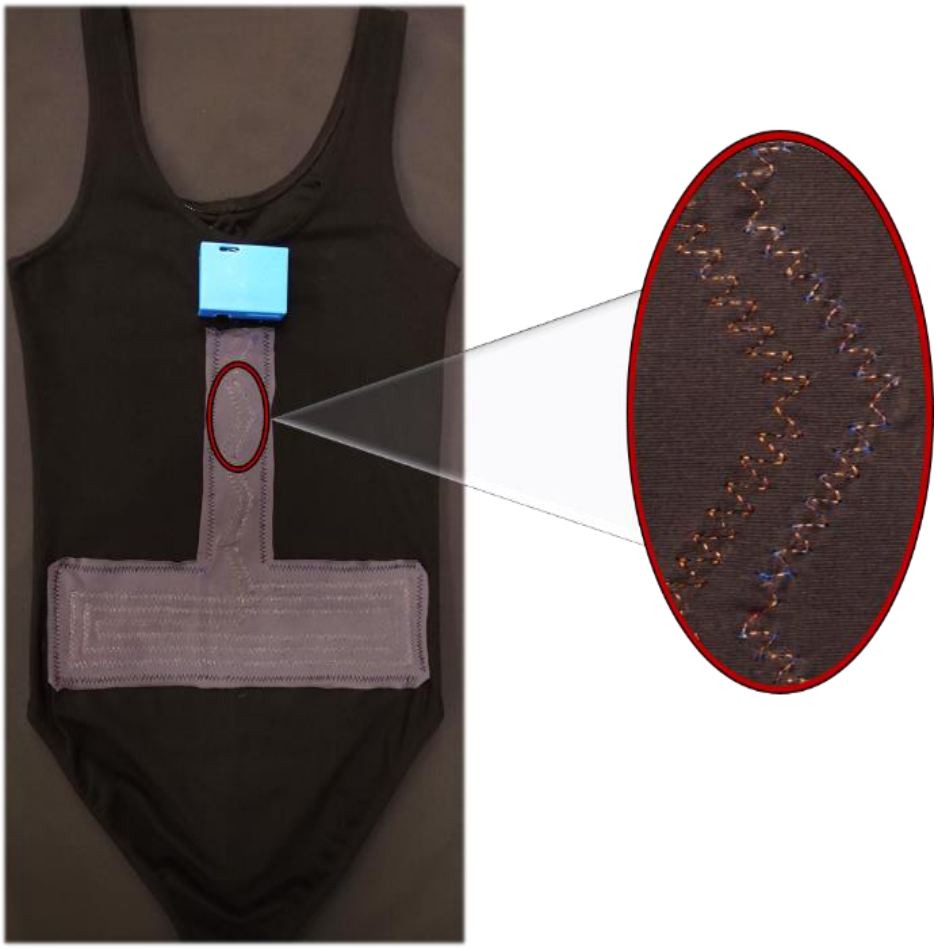

Figure 4.7 Smart garment prototype. Rear view of the smart garment with the inductive sensor affixed to the part that goes on the lumbar section. This image is licensed under a Creative Commons Attribution license (CC BY). Source image: A. G. Patiño, M. Khoshnam, and C. Menon, "Wearable device to monitor back movements using an inductive textile sensor," *Sensors (Switzerland)*, vol. 20, no. 3, pp. 5–8, 2020. Avaliable online: https://www.mdpi.com/1424-8220/20/3/905. Accesses on 14/August/2020.

Wireless communication circuitry was assembly to acquire sensor readings. More specifically, a high-resolution inductance-to-digital converter board (LDC1614, Texas Instruments Inc., Dallas, Texas) collected inductance values from the sensor and transferred data to a microprocessor (Arduino Pro Mini, ATMega328, Microchip Technology, Chandler, Arizona) via the Inter-Integrated Circuit (I2C) protocol. The microcontroller then communicated with a Bluetooth module (HC-06 Bluetooth Module, Guangzhou HC Information Technology Co., Ltd., Guangzhou, China) to transmit the received data to the user's cellphone. The aforementioned components were purchased and then connected together as illustrated in Figure 4.8. The communication used between the LDC1614 and the microprocessor was Inter-Integrated Circuit (I^2C), while the communication used between the Bluetooth module and the microprocessor was Universal Asynchronous Receiver/Transmitter (UART). The inductive sensor is connected to the LDC1614 on channel 0. A smartphone application was also developed to collect the data and store it on the phone for later processing. The circuitry was powered with a LiPo battery providing 3.7 V and 1200 mAh, and the sampling rate of the prototype was 200 Hz.

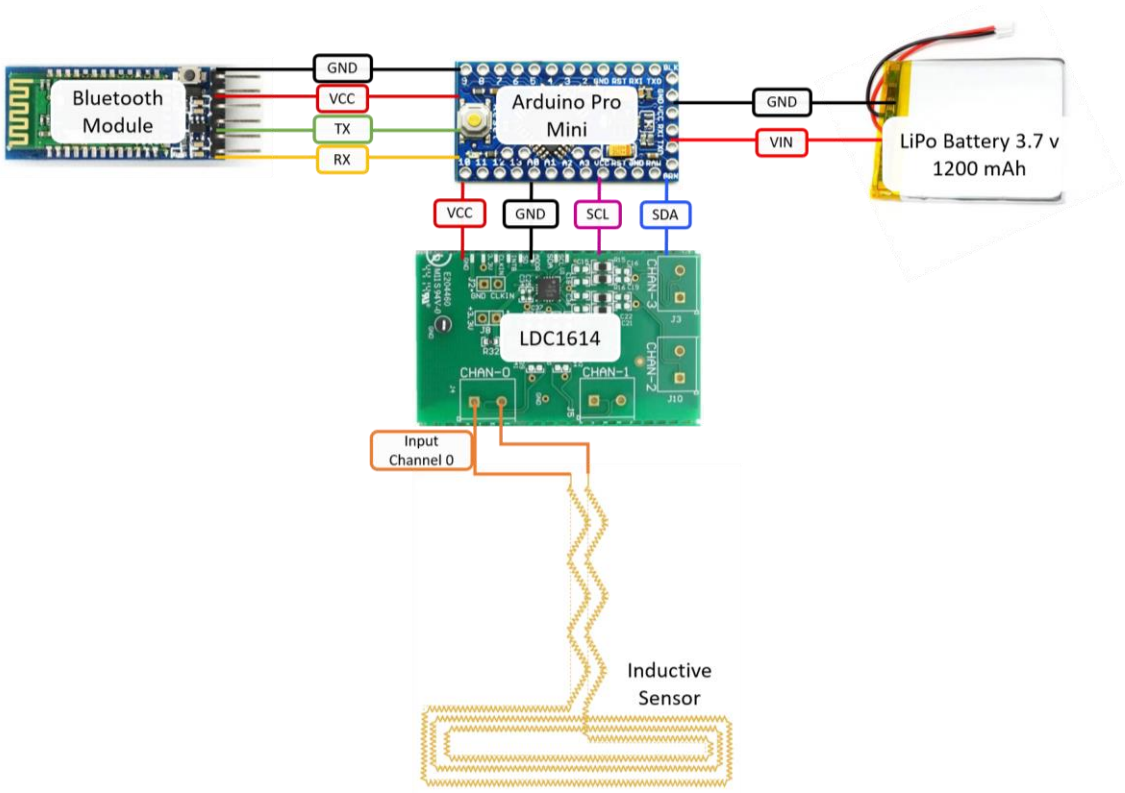

Figure 4.8 Connection diagram of the circuitry

4.3.2. Testing Protocol

To evaluate the performance of the sensor, one healthy participant (female, 25 years old, 161 cm) was asked to wear the instrumented garment and perform three cycles of the following movements:

1. Six repetitions of comfortably bending forward as much as possible at a selected speed without bending the knees;

2. Three repetitions of bending to the right, standing straight, bending forward, standing straight, and then bending to the left;

3. Three repetitions of rotating the trunk to the right, standing straight, bending forward, standing straight, and then rotating the trunk to the left.

During these movements, the participant was asked to keep her hips as still as possible. Figure 4.9a shows the participant wearing the prototype while standing straight. Figure 4.9b illustrates the participant wearing the prototype while performing maximum forward bend. To determine the true forward bending angles (roll), two IMUs (Xsens Awinda, Enschede, Netherlands) were positioned on C7 and L5. The ethics for this study was approved by the Office of Research Ethics at Simon Fraser University, and the participant gave informed consent for her participation.

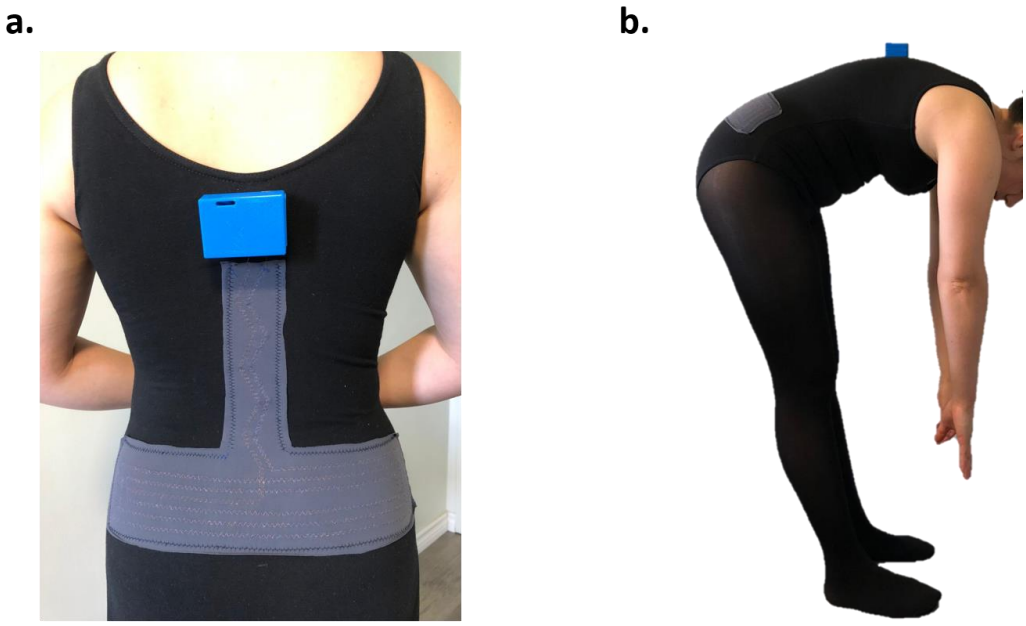

Figure 4.9 Smart garment prototype worn by the user: (a) Rear view of the smart garment when being worn by the participant; (b) participant bending forward as much as possible without bending the knees.

4.3.3. Interference Test

To investigate how the performance of the fabricated inductive sensor changes in proximity of other objects, such as magnets, metallic objects, or wireless devices, a two-phase interference test was designed:

1. In the first phase, the inductance value of the sensor was observed before and after different objects that could potentially interfere with sensor readings were brought close to the unworn garment. The chosen objects included: a copper spool (same material used for the inductive sensor with a length of 5.5 cm and a diameter of 2 cm), a disc-shaped metallic object (an alloy of iron, width = 1 cm, diameter = 3.7 cm), a disc-shaped magnet (width = 0.3 cm, diameter = 2.5 cm), a cellphone (device turned on with Wi-Fi activated), and a human hand. The prototype was fully extended on a table with the inductive sensor facing upward. The object was moved towards the inductive sensor from a distance to the proximity of the coil in the vertical direction while the largest face of the objects was facing the coil. The objects were held in the proximity of the inductive sensor for approximately 8 s.

2. In the second phase, the participant was asked to wear the prototype and perform three cycles of the following protocol:

    a. Standing upright without moving for approximately 15 s;

    b. Five repetitions of forward bending, without bending the knees as much as possible and at a comfortable speed;

    c. Picking up the phone from the table in front and putting it inside their jeans' back pocket;

    d. Standing upright without moving for approximately 25 s;

    e. Five repetitions of forward bending without bending the knees as much as possible and at a comfortable speed.

4.3.4. Outcome Measures

In evaluating the performance of the prototype fabricated with the proposed sensor design, two main outcome measurements were considered:

1. Current consumption, which is indicative of the battery life of the sensing unit. A lower current consumption allows for monitoring back movements during longer periods of time, e.g., an entire work shift,

2. Inductance value, which is the electrical response of the sensor to externally applied strains. When the user bends forward, the sensor is stretched, resulting in higher inductance values.

4.4. Experimental Results

4.4.1. Current Consumption

The power consumption of the prototype was calculated by investigating the current consumption of all the electrical components. Furthermore, an experimental test was performed by keeping the prototype active and transmitting data via Bluetooth to an external device for approximately 8 continuous hours. The experimental test was performed with the battery fully charged. The current consumption obtained from the various sensor component datasheets are as follow: the Bluetooth module consumes 8 mA when transmitting, the LDC1614 consumes 3.1 mA when active, and the microprocessor Arduino mini consumes 9 mA when active. Therefore, the prototype had a total current consumption of 20.1 mA. Considering the current consumption of the prototype and the 1200 mAh of the LiPo battery, it was possible to estimate that the prototype can operate and transmit data for approximately 59 hours. The experimental test was performed by turning on the prototype and continuously transmitting data to a cellphone via Bluetooth. The inductive sensor was stretched each hour to ensure that the data transmission was active during the entire test. After approximately 8 hours, the prototype continued to transmit data to the cellphone and operated normally.

4.4.2. Inductance Value

The inductance value of the sensor sewn on the leotard before being worn was 4.5 μH, as measured by the smart tweezers. However, the inductance value reported by the converter board was 4.6μH, which shows a difference of 2.22% between the two measurements. This comparison was performed mainly to ensure that the readings from the developed circuitry were reliable and representative of the actual inductance values.

Inductance values reported from the prototype and actual forward bending angles collected by IMUs during the testing protocol for one sample cycle of recorded movements are illustrated in Figure 4.10, in which the periods of forward bending are highlighted in grey shading. When the participant bent forward, the highest reported inductance value and the corresponding flexion angle were 5.245 μH and 40.911°, respectively. In the standing upright position, the inductance was measured at 5.036 μH at a flexion degree of -4.602° (Figure 4.10a). It is also worthwhile noting that when the bent position was held over longer periods of time, the readings of the sensor remained stable. This point is highlighted by observing Figure 4.10a; the second peak of the shown signal refers to a bent position held for over 10 s. The measured inductance value, i.e., the amplitude of the signal during this time is stable and approximately 5.225 μH, which is similar to the signal amplitude during other peaks corresponding to holding a bent position for shorter times (about 3 s).

Figure 4.10b shows results for the case in which the participant was repeating a series of forward and lateral bending movements. While the inductance values in forward bending were well above 5.1 μH, the highest inductance value in lateral bending was 5.073 μH (Figure 4.10b). A similar situation is observed in Figure 4.10c, where the inductance value during truck rotation did not go above 5.023 μH.

It is also worthwhile noting that during these tests the designed sensor demonstrated good consistency with respect to its inductance value. As observed from Figure 4.10, when the person was standing straight, the inductance stayed at a level of 5.050 μH. Similarly,

the inductance signal maintained a level of 5.230 μH during the time period that the maximum forward bent was held.

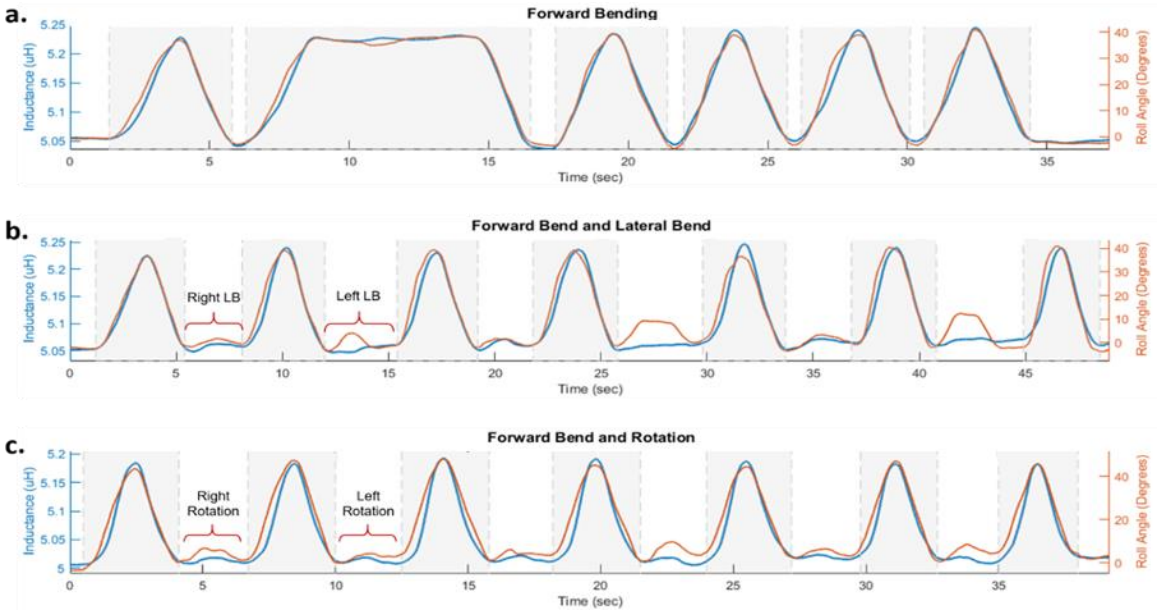

Figure 4.10 Inductance values (μH) recorded from the designed sensor and actual forward bending angles (degrees) recorded by IMUs during the considered trunk movements: (a) forward bending; (b) forward and lateral bending; (c) forward bending and trunk rotation. In each case, the periods of forward bending are highlighted in grey shading. This image is licensed under a Creative Commons Attribution license (CC BY). Source image: A. G. Patiño, M. Khoshnam, and C. Menon, "Wearable device to monitor back movements using an inductive textile sensor," *Sensors (Switzerland)*, vol. 20, no. 3, pp. 5–8, 2020. Avaliable online: https://www.mdpi.com/1424-8220/20/3/905. Accesses on 14/August/2020.

4.4.3. Comparison of Simulation and Experimental Results

The highlights of how the simulation and experimental results compared are summarized here. The inductance value of the sensor before stretching was 4.500 μH in the experimental evaluation versus 4.698 μH in the simulations. This difference of 4.4% might be due to small differences between the simulation and actual parameters since the

inductive textile sensor was manufactured by hand. The maximum inductance value during forward bending was expected to be 5.110 μH from simulations, while a value of 5.245 μH was obtained in the experiments; indicating a small difference of 2.64%, which might be due to small changes in the zigzag shape when stretched.

Since the focus of this study was on detecting forward bending movements and distinguishing them from lateral bending and twisting of the trunk, the performance of the sensor was only simulated during forward bending. Experimental evaluation of the sensor in lateral bending and twisting was carried out to better highlight how the placement of the sensor and its design and configuration resulted in a prominent sensor response during forward bending.

4.4.4. Results of the Interference Test

The results of the first phase of the interference test, i.e., when the unworn prototype was extended on the table, are shown in Figure 4.11, in which the periods of moving different objects towards the inductive sensor's coil are highlighted in gray shading.

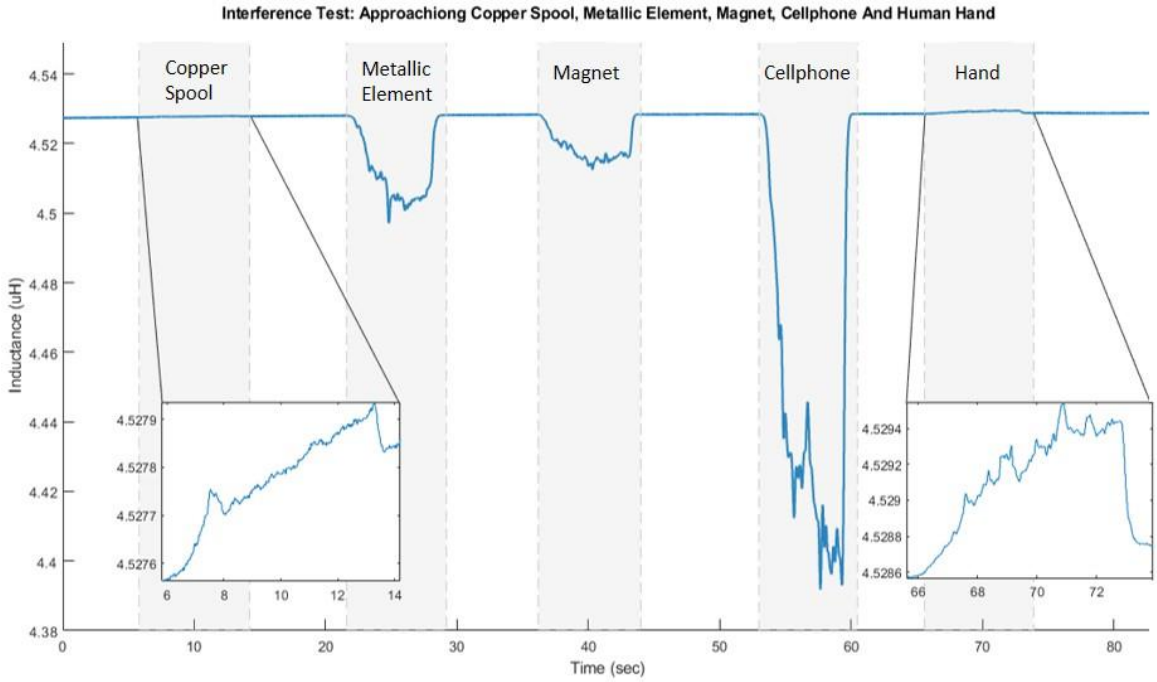

Figure 4.11 Inductance values (μH) were recorded from the interference test, where a

copper spool, a metallic element, a magnet, a cellphone, and a human hand were moved towards the inductive sensor's coil. In each case, the periods of moving objects toward the coil are highlighted in grey shading. This image is licensed under a Creative Commons Attribution license (CC BY). Source image: A. G. Patiño, M. Khoshnam, and C. Menon, "Wearable device to monitor back movements using an inductive textile sensor," *Sensors (Switzerland)*, vol. 20, no. 3, pp. 5–8, 2020. Avaliable online: https://www.mdpi.com/1424-8220/20/3/905. Accesses on 14/August/2020.

The inductive sensor values were not affected when approached by the copper spool and the human hand (first and last objects). More specifically, the maximum inductance change was 0.0003 μH (less than 0.01%) for the copper spool and 0.001 μH (about 0.02%) for the human hand. Moving the metallic element and the magnet towards the coil caused a maximum change of 0.030 μH (less than 1%) and 0.015 μH (less than 0.5%) in sensor readings, respectively. The object that interfered most with the inductive sensor was the cellphone with a maximum inductance change of 0.136 μH (about 3%). During this test, the cellphone was on, and the Wi-Fi was activated. The cellphone case almost touched the sensor.

It is worth noting that as observed in Figure 4.11, the metallic element, the magnet, and the cellphone decreased the inductance value, while the copper spool and the human hand increased it. In the case of the copper spool, such a result might be related to both elements (the copper spool and the inductive sensor) being composed of the same material. The increase in the inductance value when a human hand approached the coil might be the result of a small stimulation of excitable tissues of the hand. The inductance changes due to the hand approaching the coil were neglectable, possibly due to the similarity between the relative magnetic permeability between biological tissues and a vacuum [74]. Additionally, the inductance change between the beginning and the end of the test was 0.002 μH (about 0.04%).

Figure 4.12 illustrates the results of phase 2 of the interference test when the participant was wearing the prototype. The periods highlight in gray shading represent forward bending of the participant. The red circle shows when the participant picked up the cellphone from the table in front and put it inside the back pocket of their jeans.

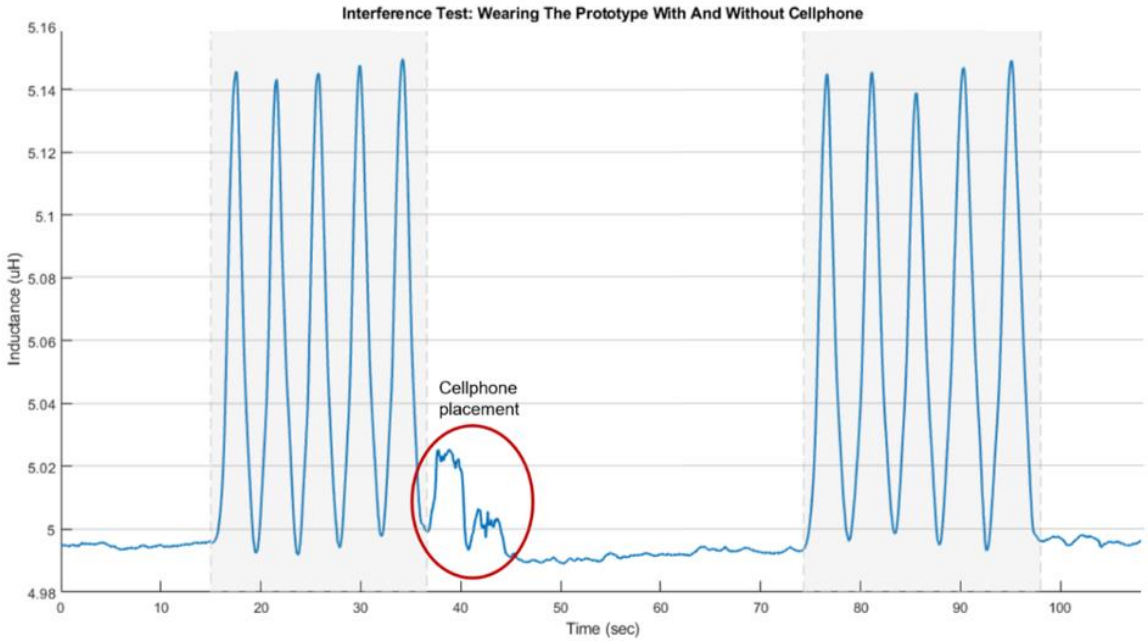

Figure 4.12 Inductance values (μH) recorded from the interference test, where a single participant was wearing the prototype and performed forward bending. In the second set of forward bend, the participant had the cellphone inside their jeans' back pocket. In each case, the periods of forward bending are highlighted in grey shading. The red circle shows when the cellphone was put inside the back pocket. This image is licensed under a Creative Commons Attribution license (CC BY). Source image: A. G. Patiño, M. Khoshnam, and C. Menon, "Wearable device to monitor back movements using an inductive textile sensor," *Sensors (Switzerland)*, vol. 20, no. 3, pp. 5–8, 2020. Avaliable online: https://www.mdpi.com/1424-8220/20/3/905. Accesses on 14/August/2020.

Although the cellphone caused the highest interference with sensor readings when the prototype was not worn (Figure 4.11), Figure 4.12 shows that the performance of the worn prototype was not affected. Periods of forward bending can be easily detected by observing the inductance values. Nevertheless, it should be noted that a decrease in the

inductance value before and after putting the cellphone in the back pocket was observed when the user was standing upright. More specifically, the sensor reading decreased from 4.994 μH to 4.992 μH (about 0.04%).

The average change in the inductance value between standing straight and bending forward, before and after placing the cellphone in the back pocket was 0.151 μH and 0.149 μH, respectively. Therefore, the interference caused by handling the cellphone while wearing the prototype affected the signal amplitude by 1.325%. It should also be noted that although, as seen in Figure 4.11, moving the cellphone towards the unworn sensor noticeably decreased the inductance value, handling the cellphone while wearing the garment had a different effect. More specifically, in this case, as observed from Figure 4.12, moving the cellphone to the back pocket resulted in a transient increase in sensor readings. However, this increase was less than 15% of the peak inductance value corresponding to the forward bending state. Therefore, the performance of the sensor in detecting forward bends was not affected by handling the cellphone in the tested scenario.

The red circle in Figure 4.12 denotes the moment when the user bends forward to pick up the cellphone from the table in front and put it inside of their jean's back pocket. It can be seen that such an action had a transient effect on the sensor readings. For this test, the back pocket was chosen to recreate a more realistic scenario and also to place the cell phone in closer proximity of the sensor's coil.

4.5. Discussion

This chapter presented an inductive sensor-based wearable garment for monitoring back movements. The fabricated prototype was comfortable, portable, and has low power consumption. Low power consumption allowed operation over longer periods of time, and was well-suited for monitoring the back movements of users during work shifts. Textile sensors have been used in the past to monitor motion and acceleration of limbs, applied pressure and/or strain, and biosignals, such as ECG signals, EEG signals, and

respiration. Fleury et al. summarized and reported different types and applications of textile sensors in healthcare, emotion monitoring, rehabilitation, and diagnosis of sleep disorders [26]. While there are very few prototypes that fully integrate the sensing elements, wiring, and power supply into the textile, the majority of the proposed solutions implement partial integration in which only the sensing elements and wiring are embedded in the fabric [26]. The prototype presented in this chapter had the inductive sensor sewn into the garment and the circuitry, including the power supply, which was affixed to the garment using Velcro.

Table 4.3 provides a comparison between specifications of the prototype presented in this paper and those of similar ones in the literature that reported similar measurements. From Table 4.3, it is observed that the present prototype is lighter than its competitors. Being lightweight is an important factor for wearable devices since it directly affects the comfort for the user [35]. Power consumption is another important feature which determines the operating life of the wearable device. Table 4.3 shows that the prototype presented by Dionisi et al. [35] has the lowest current consumption, which might be partially due to the solar panel placed on the user's back. However, this solution might not be effective when monitoring for long hours, indoors, or away from the sun. The prototype presented in our study has a higher current consumption, i.e., 20.1 mA, but using a 3.7 V battery allows the device to work for more than 8 continuous hours, which is sufficient for monitoring bending movements during an entire work shift.

Table 4.3. Comparison of the present prototype against others in the literature. This picture is licensed under a Creative Commons Attribution license (CC BY). Source image: A. G. Patiño, M. Khoshnam, and C. Menon, "Wearable device to monitor back movements using an inductive textile sensor," *Sensors (Switzerland)*, vol. 20, no. 3, pp. 5–8, 2020. Avaliable online: https://www.mdpi.com/1424-8220/20/3/905. Accesses on 14/August/2020.

Author	Type of Sensor	Integration into the Garment	Number of sensors	Recognized Movements	Wireless	Power Consumption (mA)	Weight (g)
García Patiño, A. *et al.* [75]	Inductive	Sewn	1	Forward Bend	Yes	20.1	78.6 (Circuitry and sensor)
Rezaei, A. et al [30]	Resistive	Sewn	18	Forward Bend Lateral Bend Rotation	No	Not specified	Not specified
Esfahani, M. I. M. et al. [31]	Resistive	Printed	12	Forward Bend Lateral Bend Rotation Mixed Movements	No	Not specified	≤ 200 (Sensors and garment)
Dionisi, A. et al. [35]	Textile Electrocardiography Electrodes (ECG) Inductive sensor (Plethysmography) 1 Accelerometer (Posture Monitoring)	Sewn (Textile Electrodes and Inductive sensor) Pocket and snap buttons (Circuit board) Not specified (Solar Panel)	2 Textile Electrodes 1 Inductive sensor 1 Accelerometer 1 Solar panel	Forward Fall Back Fall Right and Left Imbalance	Yes	9.6 (approx.)	81 approx. (solar panel and circuitry)
Tormene, P. et al. [32]	Resistive	Printed	13	Forward Bend Lateral Bend	Yes	Not specified	Not specified
Mattmann, C. [33]	Resistive	Silicone Film	21	Forward Bend Lateral Bend Rotation Lifting Shoulders Slumped Force Upright Arm Postures	Yes	Not specified	Not specified

Mattmann tested the proposed device for a larger set of movement types, but reported that the device could not differentiate between similar postures and that the accuracy of detecting different postures dropped from 97% to 65% when testing with a new user [33]. Tormene et al. concluded that their prototype was able to monitor forward, but not lateral bending and proposed the placement of additional sensors [32]. Rezaei et al. proposed a

wearable garment for monitoring three-dimensional movements of the trunk [30]. In addition to the higher number of resistive sensors used in that prototype, the calibration was a tedious step involving implementing a machine-learning algorithm to train a model for detecting different postures [30]. The prototype presented in this paper used a single sensor to monitor forward bending and to distinguish it from lateral bending or twisting without requiring a lengthy calibration step. It is also worth noting that while previous studies that used a tightfitting shirt or a T-shirt identified sliding of the clothing on the human body as one limitation that might lead to errors in detecting trunk postures [30], [31], [33], [35]. Dionisi et al. [35] developed a smart garment where the circuitry was attached to a T-shirt. This study reported that the weight of the solar panel pulled down the shirt causing unwanted dynamic acceleration. Moreover, Dionisi et al. [35] mentioned that the unwanted movement of the shirt caused noise in the accelerometers' output signal. To prevent the sliding Rezaei et al. [30] anchored the shirt to the person's shorts with Velcro patches. Similar to Tormene et al. [32] a smart garment using a leotard was created in this thesis, which help prevent sliding of the sensors and kept them in their original position. The leotard is a comfortable, stretchable and tightfitting garment that can be worn under the user's clothes allowing the user to move freely without interfering with their performance of activities of daily living. Furthermore, tightfitting garments allow for closely monitoring back movement while minimizing sliding of the clothes, input noise, and misreading.

The readings of the inductive textile sensor were noticeably affected when a cellphone was moved toward the unworn sensor's coil. However, the performance of the prototype was not affected when the participant wore the prototype and performed forward bending with a cellphone inside the back pocket of their jeans. Further investigation is needed to evaluate the possible interference and performance of the prototype in the presence of implantable devices and medical equipment in the hospital, e.g., pacemakers, defibrillators, magnetic resonance imaging (MRI), and cochlear implants.

The prototype demonstrated good accuracy in measuring inductance, as indicated by a difference of less than 3% between its readings and those of the commercially available smart tweezers. Furthermore, obtaining the same inductance value for the same bending pose during different movements point to the high precision of the developed sensing platform.

Unlike resistive textile sensors [33], the inductive sensor considered herein had no drift. Moreover, sensor readings showed little variation, demonstrated by an average value of 5.219 μH and a standard deviation of 0.0246 μH when the bent position was held. Nevertheless, the repeatability of results using the sensor should be further established by additional experiments. When the participant was standing upright, the inductance value was consistent during all tests. The slight differences observed in the inductance value when the participant was bending forward were mostly because the participant was not able to bend forward to the exact same bending position each time.

The inductive textile sensor was highly sensitive to forward bending movements, while lateral bending and twisting caused small variations in sensor readings (Figure 4.9). This result was due to the strategic design, configuration, and placement of the sensor such that forward bending movements caused a major strain on the sensor. Therefore, while previous studies have reported difficulties distinguishing between different movements while monitoring the back [32], the suggested platform successfully recognized and reported forward-bending episodes performed among other type of movements.

The zigzag pattern used in the inductive textile sensor had a significant impact on the inductance value, where without the mentioned pattern, the simulated inductance value dropped by more than 25%. Additionally, the zigzag pattern allowed embedding a non-stretchable material into a stretchable garment while preventing damage to the sensor.

The operating frequency of the sensor was calculated to be 3.46 MHz for the unworn prototype (inductance value = 4.5 μH) and 3.21 MHz for the worn prototype in a maximum forward bend (inductance value = 5.245 μH). According to the Consumer and

Clinical Radiation Protection Bureau, Health Canada [76], radiofrequency (RF) fields that are in the frequency range between 3 kHz and 300 GHz are safe for humans. The sensor developed in the present study has an operating frequency in the range of 3 MHz, therefore, it operates in the recommended safety limits. However, to fully establish its safety for prolonged human use, further investigation is required.

Since the focus of this study was to design a sensor to detect simple forward bending and to distinguish such movements from other movements such as twisting and lateral bending of the trunk, only simple isolated movements were considered in the testing scenarios. In this chapter, the participant was asked to bend forward and stand straight at her preferred comfortable speed. Further study is required to fully characterize the behavior of the sensor during complex movements and at different movement speeds. A future prototype will also have sensors added on the waist level on both sides such that it can also detect lateral bending and trunk rotation while still discriminating between these different types of movements. Finally, a reduction in the size of the circuitry could improve comfort by decreasing the weight of the prototype.

4.6. Summary

A smart garment to monitor trunk movements using an inductive textile sensor was developed. The design of the smart garment was discussed and its performance when a single user performed forward bends was evaluated. The zigzag pattern used to make the inductive sensor was validated through simulations and physical experiments. Moreover, power consumption was analyzed to ensure that the developed prototype would remain operational for long hours. An interference test was carried out to evaluate the smart garment readings when several ferromagnetic elements were in the proximity of the inductive sensor. Finally, the general performance of the smart garment against other prototypes presented in the literature was discussed. This chapter addressed the third objective of this thesis in developing a wireless and wearable device using an inductive textile sensor.

The smart garment presented in this chapter showed excellent performance in detecting forward-bending movements while ignoring lateral bending or trunk rotations. The designed inductive sensor had stable readings (no drift), little variation in readings during forward bends, an easy manufacturing process, and a long battery life. Therefore, the proposed platform is a potential solution for preventing LBP by informing the user about the amount of strain on their lower back during long hours during work shifts.

Chapter 5

Conclusion

In this thesis, the design of an inductive textile sensor was introduced and the fabricated inductive textile sensor prototype was integrated into a tight-fitting garment to monitor forward bending of the user to prevent and treat LBP.

The design of the inductive sensor was based on two parameters: 1) the anthropometric lumbar dimensions of a healthy participant, 2) the inductance behavior when sensor parameters such as height, width, perimeter, area, and the number of loops were modified. The anthropometric dimensions of the lumbar section were taken from the literature. The evaluation of the inductance was made using theoretical formulas from the literature and simulations made in Ansys 2019 R2/19.4. All simulations were static, future work should include evaluating the inductance value when a curvature in the sensor is presented without modifying the sensor dimensions. The simulations were based on a straight line instead of a zigzag pattern to simply calculations and reduce computational time. However, future work should include a mathematical model of an inductive sensor with a zigzag pattern.

The anthropometric size of the lumbar section of a healthy female of 25-40 years old was 280 mm × 100 mm. The mentioned dimensions were used to obtain the maximum possible inductance based on perimeter, area, width, and height. A comparison between simulations and theoretical results demonstrated that inductance behavior was similar in both approaches. The values reported through simulations were always higher compared to the theoretical results. Such a difference might be due to ignoring the sensor's material and its surroundings in the theoretical calculations. Results of the equation based on the perimeter and area presented were closer to those of simulations, while the equation based on height and width had a more linear behavior. Reducing either the perimeter or

the width of the sensor had a greater impact in the inductance value than the reducing area or height. These last two parameters should be considered when minimizing the size of the sensor but avoiding to greatly reduce the inductance value.

The size of 260 mm × 60 mm for the inductive textile sensor was selected since it covered 78.81% of the maximum inductance change based on the perimeter and area, and 78.79% of the maximum inductance change based on the height and width. Finally, the total number of loops for the inductive textile sensor was selected to be three, based on the size of the sensor, geometry, and comfortability.

The inductive textile sensor was integrated into a sleeveless tight-fitting leotard to monitor movements of the trunk. The integration of the inductive textile sensor was made by sewing a copper wire thread with a diameter of 0.14 mm into a stretchable garment. The optimal zigzag pattern configuration was selected based on a series of simulations in which the inductance was calculated based on the width of the zigzag and its resistance to breaking. The results showed that a zigzag with a 4 mm width had a relatively high inductance value and could be stretched up to 200% of the original length.

The simulation study demonstrated that the sensor was stretched to 104% and 132% of its original length in the horizontal and vertical direction, respectively, when a participant bent forward without flexing their knees. Furthermore, a simulation of the sensor using the stretched percentages and a zigzag pattern reported an inductance increase of 8.8%. The maximum inductance value (5.11 μH) was obtained when the participant performed a maximum forward bend. In a second simulation, the unstretched sensor showed a decrease of 35% in its inductance value when the zigzag pattern was removed. This result highlighted the importance of the zigzag pattern in increasing the sensitivity of the sensor. Additionally, the zigzag pattern prevented the rupture of the sensor when the garment was stretch.

The developed smart garment used wireless communication and had a relatively low power consumption of 20.1 mA. The smart garment was capable of continuously

operating and transmitting data for at least 8 h. The sampling rate of the smart garment was 200 Hz. The smart garment was capable of measuring the inductance with an error of 2.22% when compared with data from the smart tweezers (LCR Pro1, LCR Research, Toronto, Ontario, Canada).

For the experimental evaluation, a single female participant was asked to perform forward bending, lateral bending, and rotation while wearing the smart garment. In all tests, the smart garment demonstrated consistent performance with respect to its inductance value. While the participant was standing straight, the inductance value stayed at 5.050 μH. Moreover, when the participant was bending forward and maintaining her posture, the inductance was 5.230 μH. The smart garment was also able to detect forward bending while overlooking twisting and lateral bending. The interference test showed that the smart garment was more sensitive to cellphone interference (about 3%) compared to the other materials. However, this interference did not affect the performance of the smart garment when the cellphone was held close to the inductive sensor.

In conclusion, the inductive textile sensor-based wearable platform presented in chapter 4 of this study showed excellent performance in detecting forward-bending movements, while ignoring lateral bending or trunk rotations. The designed inductive sensor had stable readings (limited drift), little variations in readings during forward bends, an easy manufacturing process, and a battery life of at least 8 continuous hours. Therefore, the proposed platform is a potential solution for preventing LBP by informing the user about the amount of strain on their lower back during long hours of work shifts.

Bibliography

[1] M. Nourollahi, D. Afshari, and I. Dianat, "Awkward trunk postures and their relationship with low back pain in hospital nurses," *Work*, vol. 59, no. 3, pp. 317–323, 2018.

[2] T. Videman, A. Ojajärvi, H. Riihimäki, and J. D. G. Troup, "Low back pain among nurses: A follow-up beginning at entry to the nursing school," *Spine (Phila. Pa. 1976).*, vol. 30, no. 20, pp. 2334–2341, 2005.

[3] M. Jaromi, A. Nemeth, J. Kranicz, T. Laczko, and J. Betlehem, "Treatment and ergonomics training of work-related lower back pain and body posture problems for nurses," *J. Clin. Nurs.*, vol. 21, no. 11–12, pp. 1776–1784, 2012.

[4] Y. VYB, "New low back pain in nurses: work activities, work stress and sedentary lifestyle.," *J. Adv. Nurs.*, vol. 46, no. 4, pp. 430–440, 2004.

[5] W. Van Hoof, K. O'Sullivan, M. O'Keeffe, S. Verschueren, P. O'Sullivan, and W. Dankaerts, "The efficacy of interventions for low back pain in nurses: A systematic review," *Int. J. Nurs. Stud.*, vol. 77, no. October 2017, pp. 222–231, 2018.

[6] A. Nelson, G. Fragala, and N. Menzel, "Myths and Facts About Back Injuries in Nursing: The incidence rate of back injuries among nurses is more than double that among construction workers, perhaps because misperceptions persist about causes and solutions. The first in a two-part series.," *Am. J. Nurs.*, vol. 103, no. 2, pp. 32–40, 2003.

[7] J. A. Engels, J. W. van der Gulden, T. F. Senden, and B. van't Hof, "Work related risk factors for musculoskeletal complaints in the nursing profession: results of a questionnaire survey.," *Occup. Environ. Med.*, vol. 53, no. 9, pp. 636–641, 1996.

[8] E. F. Harkness, G. J. Macfarlane, E. S. Nahit, A. J. Silman, and J. McBeth, "Risk factors for new-onset low back pain amongst cohorts of newly employed workers," *Rheumatology*, vol. 42, no. 8, pp. 959–968, 2003.

[9] M. Villumsen, P. Madeleine, M. B. Jørgensen, A. Holtermann, and A. Samani, "The variability of the trunk forward bending in standing activities during work vs. leisure time," *Appl. Ergon.*, vol. 58, pp. 273–280, 2017.

[10] V. Putz-Anderson, B. Bernard, and S. Burt, "Musculoskeletal disorders and workplace factors," *… -Related Musculoskelet. …*, vol. 97–141, no. July 1997, pp. 1-1-7–11, 1997.

[11] O. Airaksinen *et al.*, "Chapter 4: European guidelines for the management of chronic nonspecific low back pain," *Eur. Spine J.*, vol. 15, no. SUPPL. 2, pp. 192–300, 2006.

[12] S. Straube *et al.*, "Back schools for the treatement of chronic low back pain _ possibility of benefit but no convincing evidende after 47 years of research-systematic review and meta-analysis.pdf," vol. 157, pp. 2160–2172, 2016.

[13] A. Murtezani, V. Govori, V. S. Meka, Z. Ibraimi, S. Rrecaj, and S. Gashi, "A comparison of McKenzie therapy with electrophysical agents for the treatment of work related low back pain: A randomized controlled trial," *J. Back Musculoskelet. Rehabil.*, vol. 28, no. 2, pp. 247–253, 2015.

[14] P. A. The and L. Spine, "McKenzie Method of Mechanical Diagnosis and Therapy," 2014. [Online]. Available: http://www.mckenzieinstitute.org/clinicians/mckenzie-method/.

[15] D. Steffens *et al.*, "Prevention of Low Back Pain," *JAMA Intern. Med.*, vol. 176, no. 2, pp. 199–208, 2016.

[16] O. T. Lam, D. M. Strenger, M. Chan-Fee, P. T. Pham, R. A. Preuss, and S. M. Robbins, "Effectiveness of the McKenzie Method (Mechanical Diagnosis and Therapy) for Treating Low Back Pain: Literature Review With Meta-analysis," *J. Orthop. Sport. Phys. Ther.*, vol. 48, no. 6, pp. 1–53, 2018.

[17] A. Ramond-Roquin *et al.*, "Biomechanical constraints remain major risk factors for low back pain. Results from a prospective cohort study in French male employees," *Spine J.*, vol. 15, no. 4, pp. 559–569, 2015.

[18] D. C. Ribeiro, D. Aldabe, J. H. Abbott, G. Sole, and S. Milosavljevic, "Dose-response relationship between work-related cumulative postural exposure and low back pain: A systematic review," *Ann. Occup. Hyg.*, vol. 56, no. 6, pp. 684–696, 2012.

[19] W. E. Hoogendoorn, M. N. van Poppel, P. M. Bongers, B. W. Koes, and L. M. Bouter, "Physical load during work and leisure time as risk factors for back pain," *Scand. J. Work. Environ. Heal.*, vol. 25, no. 5, pp. 387–403, 1999.

[20] J. Lagersted-Olsen, B. L. Thomsen, A. Holtermann, K. Søgaard, and M. B. Jørgensen, "Does objectively measured daily duration of forward bending predict development and aggravation of low-back pain? A prospective study," *Scand. J. Work. Environ. Heal.*, vol. 42, no. 6, pp. 528–537, 2016.

[21] M. Villumsen, A. Holtermann, A. Samani, P. Madeleine, and M. B. Jørgensen, "Social support modifies association between forward bending of the trunk and low-back pain: Cross-sectional field study of blue-collar workers," *Scand. J. Work. Environ. Heal.*, vol. 42, no. 2, pp. 125–134, 2016.

[22] M. Villumsen, A. Samani, M. B. Jørgensen, N. Gupta, P. Madeleine, and A. Holtermann, "Are forward bending of the trunk and low back pain associated among Danish blue-collar workers? A cross-sectional field study based on objective measures," *Ergonomics*, vol. 58, no. 2. Taylor & Francis, pp. 246–258, 2015.

[23] A. Nelson, J. D. Lloyd, N. Menzel, and C. Gross, "Preventing nursing back injuries: redesigning patient handling tasks.," *AAOHN J.*, vol. 51, no. 3, pp. 126–134, 2003.

[24] N. A. Nelson and R. E. Hughes, "Quantifying relationships between selected work-related risk factors and back pain: A systematic review of objective biomechanical measures and cost-related health outcomes," *Int. J. Ind. Ergon.*, vol. 39, no. 1, pp. 202–210, 2009.

[25] E. Papi, W. S. Koh, and A. H. McGregor, "Wearable technology for spine movement assessment: A systematic review," *J. Biomech.*, vol. 64, pp. 186–197, 2017.

[26] A. Fleury, M. Sugar, and T. Chau, "E-textiles in Clinical Rehabilitation: A Scoping Review," *Electronics*, vol. 4, no. 1, pp. 173–203, 2015.

[27] O. Atalay, "Textile-Based, Interdigital, Capacitive, Soft-Strain Sensor for Wearable Applications," *Materials (Basel).*, vol. 11, 2018.

[28] C. Gonçalves, A. Ferreira da Silva, J. Gomes, and R. Simoes, "Wearable E-Textile Technologies: A Review on Sensors, Actuators and Control Elements," *Inventions*, vol. 3, no. 1, p. 14, 2018.

[29] B. Trovato, G. K. M. Tobin, and L. Thorväld, "Initial Investigations into Characterizing DIY E-Textile Stretch Sensors," *STEWART, RL; Skach, S; 4th Conf. Mov. Comput.*, 2017.

[30] A. Rezaei, T. J. Cuthbert, M. Gholami, and C. Menon, "Application-based production and testing of a core–sheath fiber strain sensor for wearable electronics: Feasibility study of using the sensors in measuring tri-axial trunk motion angles," *Sensors (Switzerland)*, vol. 19, no. 19, pp. 7–10, 2019.

[31] M. I. Mokhlespour Esfahani *et al.*, "Trunk motion system (TMS) using printed body worn sensor (BWS) via data fusion approach," *Sensors (Switzerland)*, vol. 17, no. 1, 2017.

[32] P. Tormene *et al.*, "Estimation of human trunk movements by wearable strain sensors and improvement of sensor's placement on intelligent biomedical clothes," *Biomed. Eng. Online*, vol. 11, pp. 1–8, 2012.

[33] C. Mattmann, "Body posture detection using strain sensitive clothing," ETH Zurich, 2008.

[34] E. Sardini, M. Serpelloni, and M. Ometto, "Smart vest for posture monitoring in rehabilitation exercises," *2012 IEEE Sensors Appl. Symp. SAS 2012 - Proc.*, pp. 161–165, 2012.

[35] A. Dionisi, D. Marioli, E. Sardini, and M. Serpelloni, "Autonomous Wearable System for Vital Signs Measurement With Energy-Harvesting Module," *IEEE Trans. Instrum. Meas.*, vol. 65, no. 6, pp. 1423–1434, 2016.

[36] J. Coosemans, B. Hermans, and R. Puers, "Integrating wireless ECG monitoring in textiles," *Sensors Actuators, A Phys.*, vol. 130–131, no. SPEC. ISS., pp. 48–53, 2006.

[37] R. Wijesiriwardana, "Inductive fiber-meshed strain and displacement transducers for respiratory measuring systems and motion capturing systems," *IEEE Sens. J.*, vol. 6, no. 3, pp. 571–579, 2006.

[38] H. R. Koo *et al.*, "The effect of textile-based inductive coil sensor positions for heart rate monitoring," *J. Med. Syst.*, vol. 38, no. 2, 2014.

[39] M. Tavassolian, T. J. Cuthbert, C. Napier, J. Peng, and C. Menon, "Textile-Based Inductive Soft Strain Sensors for Fast Frequency Movement and Their Application in Wearable Devices Measuring Multiaxial Hip Joint Angles during Running," *Adv. Intell. Syst.*, vol. 2, no. 4, p. 1900165, 2020.

[40] H. J. Yoo, "Your heart on your sleeve: Advances in textile-based electronics are weaving computers right into the clothes we wear," *IEEE Solid-State Circuits Mag.*, vol. 5, no. 1, pp. 59–70, 2013.

[41] O. Atalay, W. Richard Kennon, and M. Dawood Husain, "Textile-based weft knitted strain sensors: Effect of fabric parameters on sensor properties," *Sensors (Switzerland)*, vol. 13, no. 8, pp. 11114–11127, 2013.

[42] G. Zhou *et al.*, "Highly Sensitive Wearable Textile-Based Humidity Sensor Made

of High-Strength, Single-Walled Carbon Nanotube/Poly(vinyl alcohol) Filaments," *ACS Appl. Mater. Interfaces*, vol. 9, no. 5, pp. 4788–4797, 2017.

[43] O. Atalay, A. Tuncay, M. D. Husain, and W. R. Kennon, "Comparative study of the weft-knitted strain sensors," *J. Ind. Text.*, vol. 46, no. 5, pp. 1212–1240, 2017.

[44] S. R. Kim, J. H. Kim, and J. W. Park, "Wearable and Transparent Capacitive Strain Sensor with High Sensitivity Based on Patterned Ag Nanowire Networks," *ACS Appl. Mater. Interfaces*, vol. 9, no. 31, pp. 26407–26416, 2017.

[45] M. Pacelli, L. Caldani, and R. Paradiso, "Textile piezoresistive sensors for biomechanical variables monitoring," *Annu. Int. Conf. IEEE Eng. Med. Biol. - Proc.*, pp. 5358–5361, 2006.

[46] T.-H. Huang *et al.*, "A Novel Design of E-Textile Integration for Physiological Monitoring and Lighting," *J. Fash. Text. Eng.*, pp. 4–7, 2018.

[47] X. Liao *et al.*, "Flexible and highly sensitive strain sensors fabricated by pencil drawn for wearable monitor," *Adv. Funct. Mater.*, vol. 25, no. 16, pp. 2395–2401, 2015.

[48] M. Gholami, A. Rezaei, T. J. Cuthbert, C. Napier, and C. Menon, "Lower body kinematics monitoring in running using fabric-based wearable sensors and deep convolutional neural networks," *Sensors (Switzerland)*, vol. 19, no. 23, 2019.

[49] J. Shintake, E. Piskarev, S. H. Jeong, and D. Floreano, "Ultrastretchable Strain Sensors Using Carbon Black-Filled Elastomer Composites and Comparison of Capacitive Versus Resistive Sensors," *Adv. Mater. Technol.*, vol. 3, no. 3, pp. 1–8, 2018.

[50] A. Chhetry, H. Yoon, and J. Y. Park, "A flexible and highly sensitive capacitive pressure sensor based on conductive fibers with a microporous dielectric for wearable electronics," *J. Mater. Chem. C*, vol. 5, no. 38, pp. 10068–10076, 2017.

[51] C. B. Cooper *et al.*, "Stretchable Capacitive Sensors of Torsion, Strain, and Touch Using Double Helix Liquid Metal Fibers," *Adv. Funct. Mater.*, vol. 27, no. 20, 2017.

[52] J. O. Fava, L. Lanzani, and M. C. Ruch, "Multilayer planar rectangular coils for eddy current testing: Design considerations," *NDT E Int.*, vol. 42, no. 8, pp. 713–720, 2009.

[53] P. Martinot-Lagarde, R. Sartene, M. Mathieu, and G. Durand, "What does inductance plethysmography really measure?," *J. Appl. Physiol.*, vol. 64, no. 4, pp.

1749–1756, 1988.

[54] M. Catrysse, R. Puers, C. Hertleer, L. Van Langenhove, H. Van Egmond, and D. Matthys, "Towards the integration of textile sensors in a wireless monitoring suit," *Sensors Actuators, A Phys.*, vol. 114, no. 2–3, pp. 302–311, 2004.

[55] J. Zhong, S. Member, A. Kiourti, and T. Sebastian, "Conformal Load - Bearing Spiral Antenna on Conductive Textile Threads," no. c, pp. 1–4, 2016.

[56] D. Wu *et al.*, "A wearable respiration monitoring system based on digital respiratory inductive plethysmography," *Proc. 31st Annu. Int. Conf. IEEE Eng. Med. Biol. Soc. Eng. Futur. Biomed. EMBC 2009*, no. June, pp. 4844–4847, 2009.

[57] Y. Huang *et al.*, "Self-similar design for stretchable wireless LC strain sensors," *Sensors Actuators, A Phys.*, vol. 224, pp. 36–42, 2015.

[58] B. Bonroy, K. Meijer, P. Dunias, K. Cuppens, R. Gransier, and B. Vanrumste, "Ambulatory Monitoring of Physical Activity Based on Knee Flexion/Extension Measured by Inductive Sensor Technology," *ISRN Biomed. Eng.*, vol. 2013, pp. 1–10, 2013.

[59] N. Luo *et al.*, "Textile-Enabled Highly Reproducible Flexible Pressure Sensors for Cardiovascular Monitoring," *Adv. Mater. Technol.*, vol. 3, no. 1, pp. 1–8, 2018.

[60] Paradiso R, Loriga G, and Taccini N., "A wearable health care system based on knitted," *IEEE Trans. Inf. Technol. Biomed.*, vol. 9, no. 3, pp. 337–344, 2005.

[61] A. Vogl, P. Parzer, T. Babic, J. Leong, A. Olwal, and M. Haller, "StretchEBand: Enabling Fabric-Based Interactions through Rapid Fabrication of Textile Stretch Sensors," *Proc. 2017 CHI Conf. Hum. Factors Comput. Syst. (CHI '17)*, pp. 2617–2627, 2017.

[62] I. T. Bjørk, G. B. Samdal, B. S. Hansen, S. Tørstad, and G. A. Hamilton, "Job satisfaction in a Norwegian population of nurses: A questionnaire survey," *Int. J. Nurs. Stud.*, vol. 44, no. 5, pp. 747–757, 2007.

[63] E. S. Castel, L. R. Ginsburg, S. Zaheer, and H. Tamim, "Understanding nurses' and physicians' fear of repercussions for reporting errors: clinician characteristics, organization demographics, or leadership factors?," *BMC Health Serv. Res.*, vol. 15, no. 1, pp. 1–10, 2015.

[64] S. Y. Ang *et al.*, "Demographics and Personality Factors Associated with Burnout among Nurses in a Singapore Tertiary Hospital," *Biomed Res. Int.*, vol. 2016, 2016.

[65] E. Churchill, L. L. Laubach, J. T. Mcconville, and I. Tebbetts, "Anthropometric source book. Volume 1: Anthropometry for Designers," *National Aeronaitics and Space Administration (NASA)*, 1978. [Online]. Available: https://msis.jsc.nasa.gov/sections/section03.htm#_3.3_ANTHROPOMETRIC_AND. [Accessed: 18-Jun-2020].

[66] M. Wang, A. B. Leger, and G. A. Dumas, "Prediction of back strength using anthropometric and strength measurements in healthy females," *Clin. Biomech.*, vol. 20, no. 7, pp. 685–692, 2005.

[67] W. S. Marras, M. J. Jorgensen, K. P. Granata, and B. Wiand, "Female and male trunk geometry: Size and prediction of the spine loading trunk muscles derived from MRI," *Clin. Biomech.*, vol. 16, no. 1, pp. 38–46, 2001.

[68] T. Podbevšek, "For a good fitted skirt, the waist-to-hip distance should be measured," *Anthropol. Notebooks*, vol. 20, no. 2, pp. 77–88, 2014.

[69] M. T. Thompson, "Inductance Calculation Techniques --- Part II: Approximations and Handbook Methods," *Power Control Intell. Motion*, p. 11, 1999.

[70] F. E. Terman, *Radio Engineers' Handbook*, First Edit. United States of America: McGraq-Hill Book Company Inc, 1943.

[71] F. W. Grover, "Methods, formulas, and tables for the calculation of antenna capacity," *Sci. Pap. Bur. Stand.*, vol. 22, p. 569, 1926.

[72] Ansoft, *Maxwell 3D Guide v11.1*, REV2.0. 2005.

[73] L. Sandrolini, U. Reggiani, and G. Puccetti, "Analytical calculation of the inductance of planar zig-zag spiral inductors," *Prog. Electromagn. Res.*, vol. 142, no. July, pp. 207–220, 2013.

[74] E. Andreozzi, G. D. Gargiulo, A. Fratini, D. Esposito, and P. Bifulco, "A contactless sensor for pacemaker pulse detection: Design hints and performance assessment," *Sensors (Switzerland)*, vol. 18, no. 8, 2018.

[75] A. G. Patiño, M. Khoshnam, and C. Menon, "Wearable device to monitor back movements using an inductive textile sensor," *Sensors (Switzerland)*, vol. 20, no. 3, pp. 5–8, 2020.

[76] H. Canada, "Limits of Human Exposure to Radiofrequency Electromagnetic Energy in the Frequency Range from 3 kHz to 300 GHz." [Online]. Available: https://www.canada.ca/en/health-canada/services/publications/health-risks-

safety/limits-human-exposure-radiofrequency-electromagnetic-energy-range-3-300.html.